

CHAPTER – 7
PHOTOCONDUCTIVITY

CHAPTER – VII

PHOTOCONDUCTIVITY

I. INTRODUCTION :

Photoconductivity processes involve absorption of energies from electromagnetic radiations (X-rays, γ -rays, UV, visible light, IR) and the excitation of charge carriers from a non-conducting ground state to a higher energy state where they are free to contribute to the electrical conductivity and the return of charge carriers from the conducting states to their ground states. These are structure sensitive phenomena depending on impurity content and structural defects in the material. All semiconductors and insulators are photoconductors. The life time of the free carriers and capture cross sections are important characteristic parameters of a photoconductor. The conductivity increases upon exposure to suitable radiation. The number of materials, for which the conductivity increases large enough and hence can be useful, is fairly very small. Whereas an ample study can be found reported in literature on the thermoelectric and other transport properties of Bi_2Te_3 , there is no report so far on photoconductivity study particularly on the doped Bi_2Te_3 thin films. The results obtained of measurements of photoconductivity of $\text{Sb}_{0.2}\text{Bi}_{1.8}\text{Te}_3$,

$\text{Sn}_{0.2}\text{Bi}_{1.8}\text{Te}_3$ and $\text{Bi}_2\text{Te}_{2.8}\text{Se}_{0.2}$ thin films carried out by the author are presented below, following a general overview of the phenomenon.

II. GENERAL DISCUSSION :

When light is absorbed by a material so as to raise electrons to higher energy states, several possibilities occur. If the excited electrons are in the conduction band, the conductivity of the material increases as a result of absorption of light and the effect is known as photoconductivity. If the excited electrons give up their excess energy in the form of photons while returning to their initial state, the effect is known as luminescence. The photocurrent (current increased by illumination) depends on the intensity and wavelength of the illuminating light and the temperature of the specimen.

Trapping is a fundamental process for energy storage in almost all electronically active solids. This energy storage is accomplished by the spatial location of an electron or hole, in such a way that the electron or hole is prohibited from moving freely through the crystal unless supplied with thermal or optical energy. When the trapped electrons or holes are released, they are free to move until captured by a recombination center or by another trap. Those regions which are able to capture electrons and holes and detain them in a restricted volume are called traps.

The capturing centres may be classified into two groups^[4]:

1. **Trapping Centre** : If the captured carrier has a greater probability of being thermally re-excited to the free state than of recombining with a carrier of opposite sign at the imperfection, the centre is called a trap centre.

2. **Recombination Centre** : If the captured carrier has a greater probability of recombining with a carrier of opposite sign, say, at the imperfection, than of being re-excited to the free state, the centre is called a recombination centre.

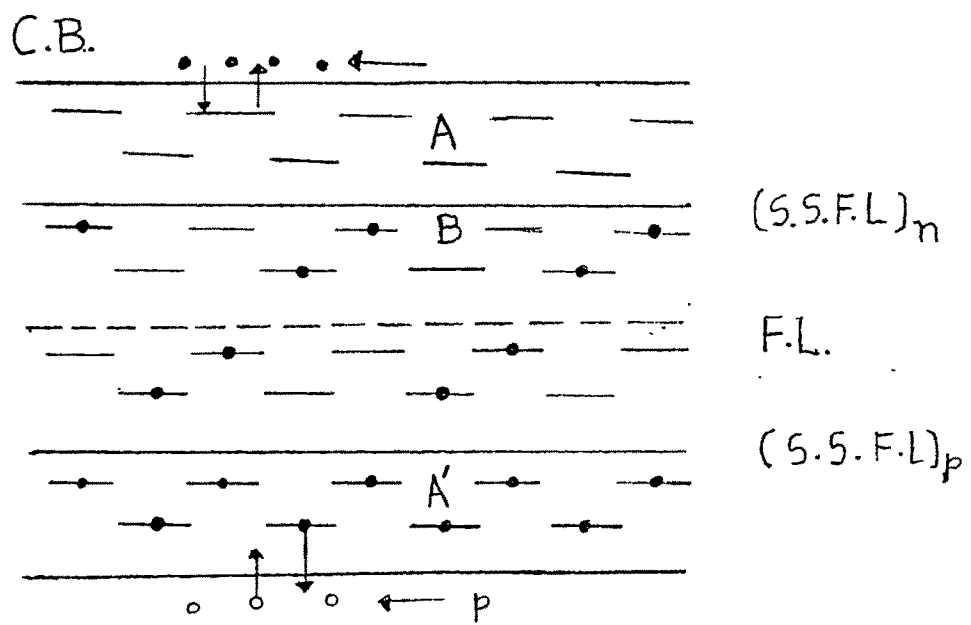
Although, a centre with an energy level lying near one of the band edges will be more likely to act as a trap than as a recombination centre (and vice versa for centres with levels lying near the middle of the forbidden gap), the distinction between traps and recombination centres is a distinction drawn on the basis of the relative probability of thermal ejection versus recombination, i.e., on kinetic conditions, and not on the basis of the intrinsic nature of the centres themselves. A recombination centre at one condition of light level and temperature may act as a trap at another condition of light level and temperature.

Recombination may also occur, as in the more usual cases, through recombination centres : either an electron being captured by an excited centre containing a hole, or a hole being captured by an excited centre containing an electron. A photoconductor quality is judged usually by photosensitivity which means photoconductivity per unit excitation intensity, i.e., the change in

conductivity caused by excitation divided by the excitation intensity.

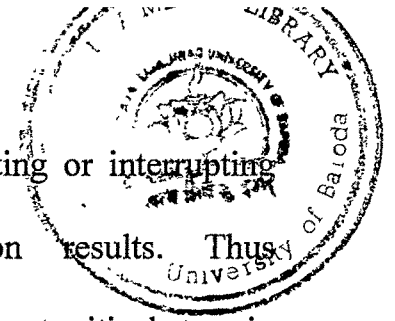
When light of appropriate wavelength is incident on a photoconductor free electrons and holes are generated at identical rates and recombine via the discrete states (impurity levels) (Figure - 1). On physical grounds it can be stated that there are states (A) near the conduction band and above steady state electron Fermi level such that the electrons falling into these states are rapidly re-excited thermally into the conduction band. These states which are in thermal equilibrium with the electrons in the conduction band are known as shallow trapping states. It is also clear that the electron falling into deeper lying states (B) will not be thermally re-excited for a long time. Before thermal re-excitation takes place, such an electron is more likely to capture a free hole. These deeper lying states are known as ground states (recombination centres). The electrons and holes falling into these states have completed their life history. The occupancy of ground states by electrons or holes is determined by purely kinetic processes of recombination. The occupancy of shallow trapping states is determined by the condition of being in thermal equilibrium with the electrons in the conduction band or the holes in the filled band.

Bube^[2] has conveniently defined the location of a demarcation level, separating the trapping and the re-combination levels with a more intricate picture of distribution of states.



V.B.

Fig. 1.



When the recombination or capture process terminating or interrupting photoconductivity is radiative, luminescence emission results. Thus measurements of luminescence provide useful information about critical steps in the mechanism of photoconductivity.

According to the Scharnhorst model^[3] the temperature dependence of photoconductivity is through

$$\Delta\sigma(T) \propto \mu_0 n_0(T) = \mu \Delta n \quad \dots\dots 1$$

The maxima in $\Delta\sigma(T)$ will be observed regardless of the magnitude of the fixed intensity of illumination, (where Δn is the excess electron density, n_0 is the equilibrium electron density, μ is the carrier mobility and Δ photoconductivity).

Rose^[4] explained the photoconductivity dependence on intensity and temperature on the basis of the concept of electron and hole demarcation levels mentioned above. The recombination velocity is governed by the discrete states lying between the two demarcation levels. Discrete states lying outside the two demarcation lines have a negligible effect on recombination. The positions of demarcation lines usually coincide almost exactly with steady state Fermi levels or the quasi-Fermi levels, the portions of which in turn determine the electron and hole densities in the bands. When the rate of generation of non-equilibrium carriers increases, their densities in the band increases and the quasi-Fermi levels are displaced towards the band edges. Consequently, the levels which

have acted as traps under weak excitation now become recombination centres. Conversely, when the generation of non-equilibrium carriers is reduced, their density decreases and the quasi-Fermi levels approach one another coming close to the equilibrium position. Then the levels which have acted as recombination levels under intense excitation become traps.

In the case of weak excitation, when the free carrier densities are low compared to the densities of band electrons and holes, the total densities of bound carriers remain practically constant. However, the localized electrons and holes are re-distributed between recombination and trapping levels by intermediate transitions to the bands and from bands to these levels.

III. Experimental Results :

Thin films of $\text{Sb}_{0.2}\text{Bi}_{1.8}\text{Te}_3$, $\text{Sn}_{0.2}\text{Bi}_{1.8}\text{Te}_3$ and $\text{Bi}_2\text{Te}_{2.8}\text{Se}_{0.2}$ were prepared on cleaned glass substrates at room temperature ($\sim 313\text{K}$) using the thermal evaporation method under a pressure of 10^{-5} Pa. 180 nm, 190nm and 210 nm thick films of these materials were obtained. Aluminum film electrodes with finger shape geometry were deposited on the films, as shown in Figure-2. This particular geometry of the electrode enables a large sensitivity area to be employed between closely spaced electrodes and hence increases the sensitivity. The photoconductivity of these films was measured as a function of illumination

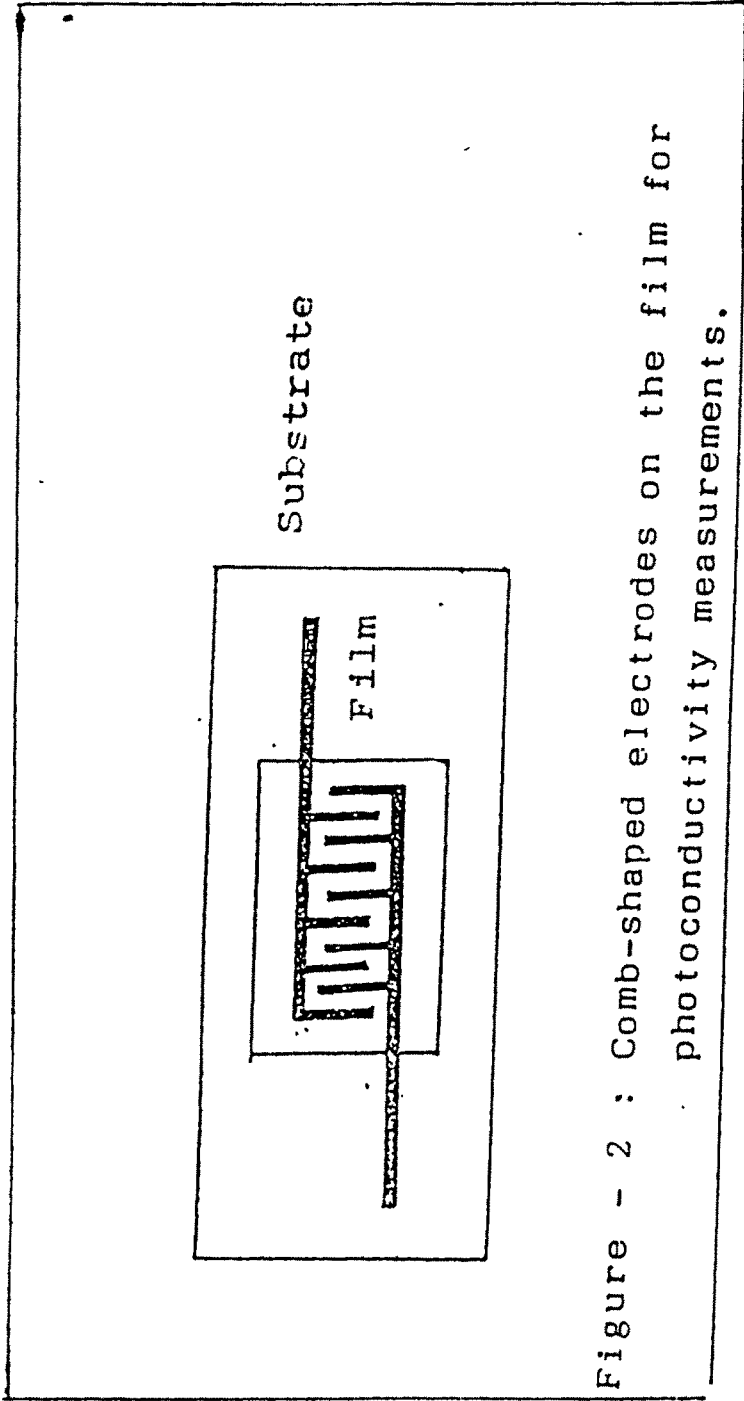


Figure - 2 : Comb-shaped electrodes on the film for photoconductivity measurements.

time, intensity and temperature. The illumination source was a 750 watt halogen lamp. The intensity was measured by a foot-candle meter and converted into units of lux. The photocurrent was measured by a microammeter. For higher temperature studies, the sample was kept inside the vacuum chamber (10^{-5} Pa.) to prevent oxidation. As in the conductivity experiment, radiant heater and chromel-Alumel thermo-couple were used for heating and measuring the temperature, respectively.

Variation of Photocurrent with intensity :

Variation of logarithm of photocurrent (which is the difference of currents obtained under illumination and under darkness) with light intensity, obtained for $\text{Sb}_{0.2} \text{Bi}_{1.8} \text{Te}_3$, $\text{Sn}_{0.2} \text{Bi}_{1.8} \text{Te}_3$ and $\text{Bi}_2 \text{Te}_{2.8} \text{Se}_{0.2}$ thin films is as displayed in Figures 3 (a),(b) and (c), respectively (i.e. $\text{Log } \Delta\sigma \text{ Vs Log } L$). The readings were taken at room temperature. The light intensity was varied from 150 lux to about 800 lux . It can be seen that there is a change in the slopes of the straight lines, observed in all the three cases at a light intensity of around 646 lux . The slope values n are indicated near the respective regions in the plot. Similar changes have been reported in a number of semiconductor films ^[5-8] .

This change corresponds to a change involving the behaviour of a centre, from that of a trap to that of a recombination centre with change in intensity. If

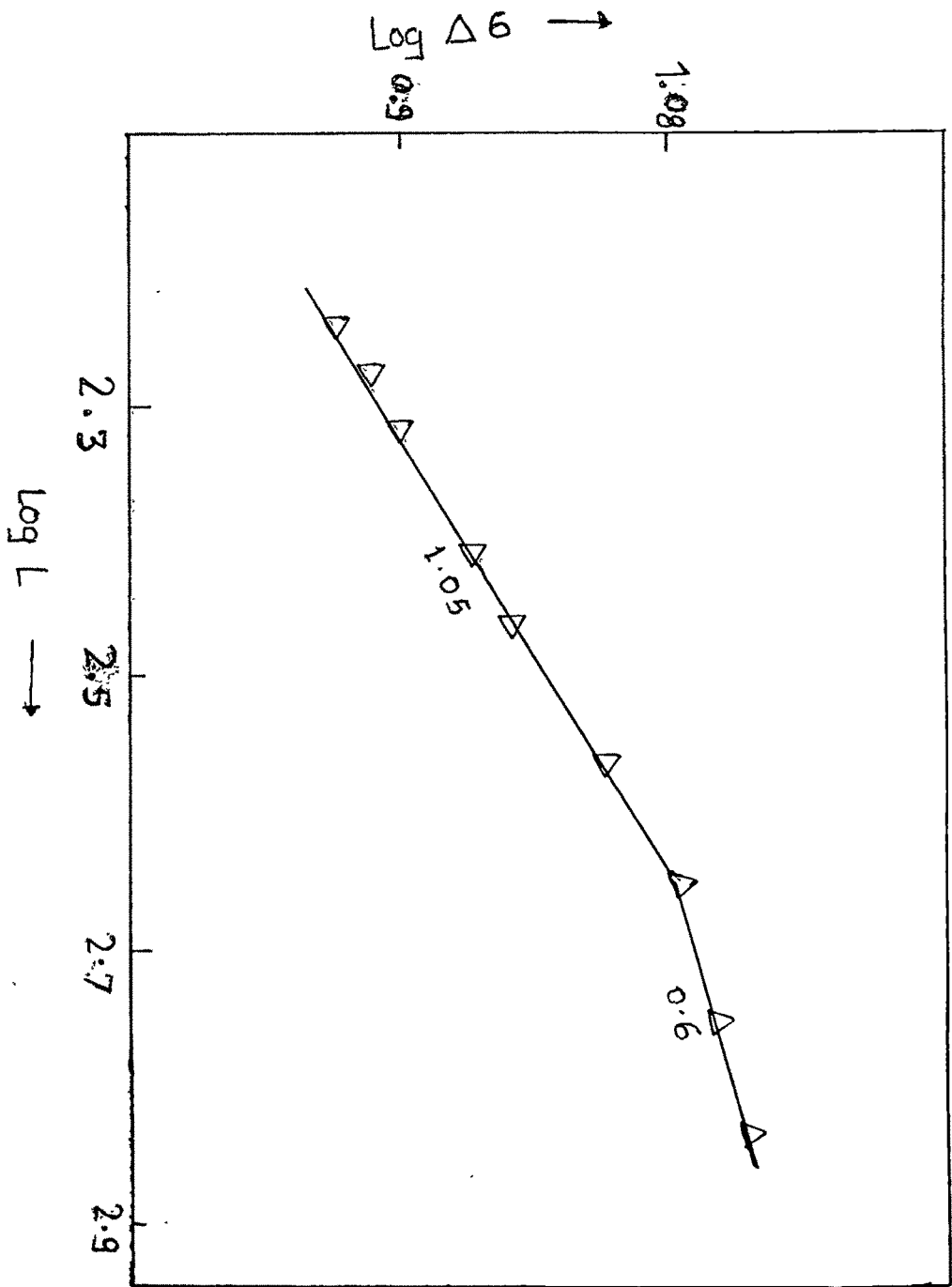


Fig. 3(a)

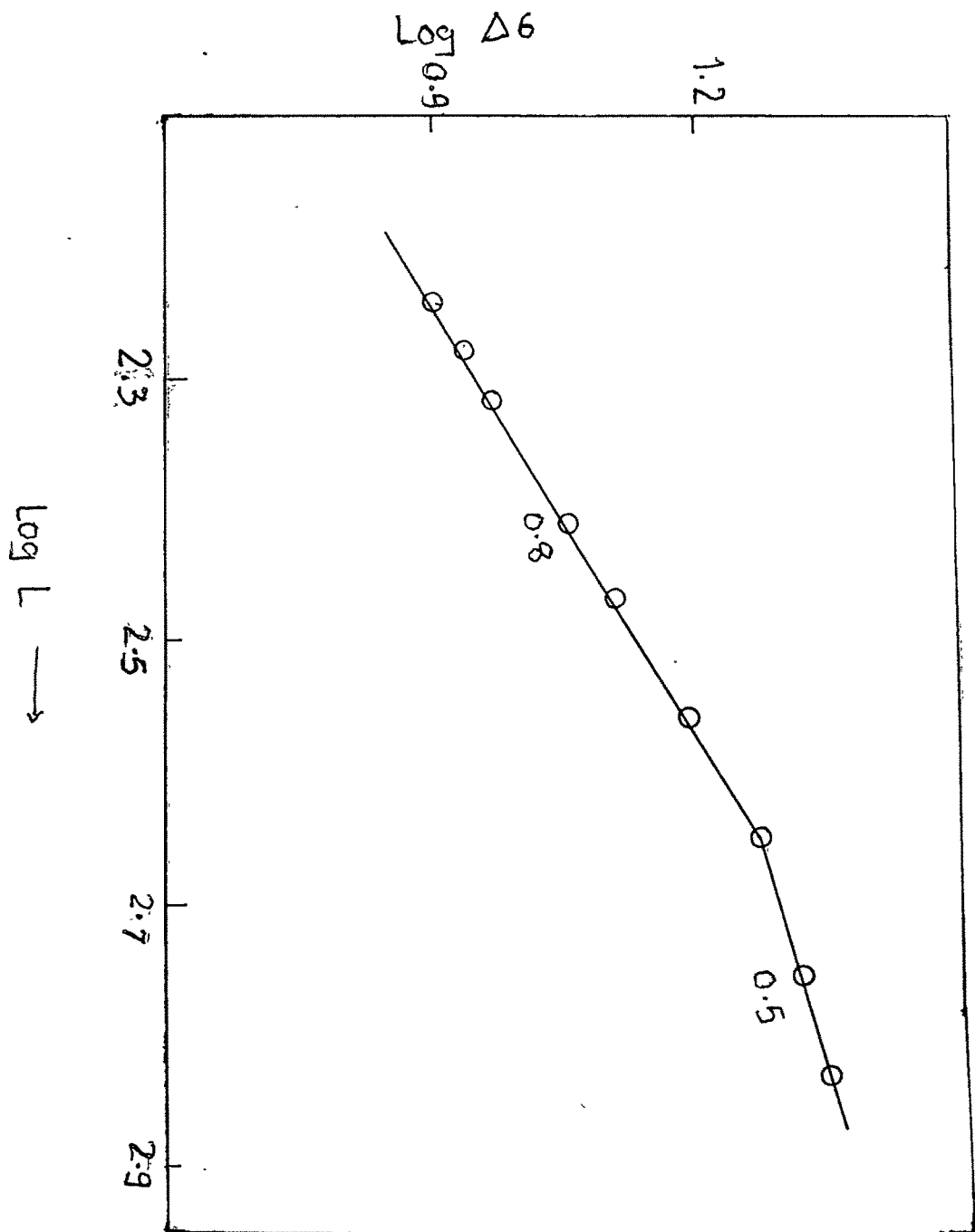


Fig. 3[b]

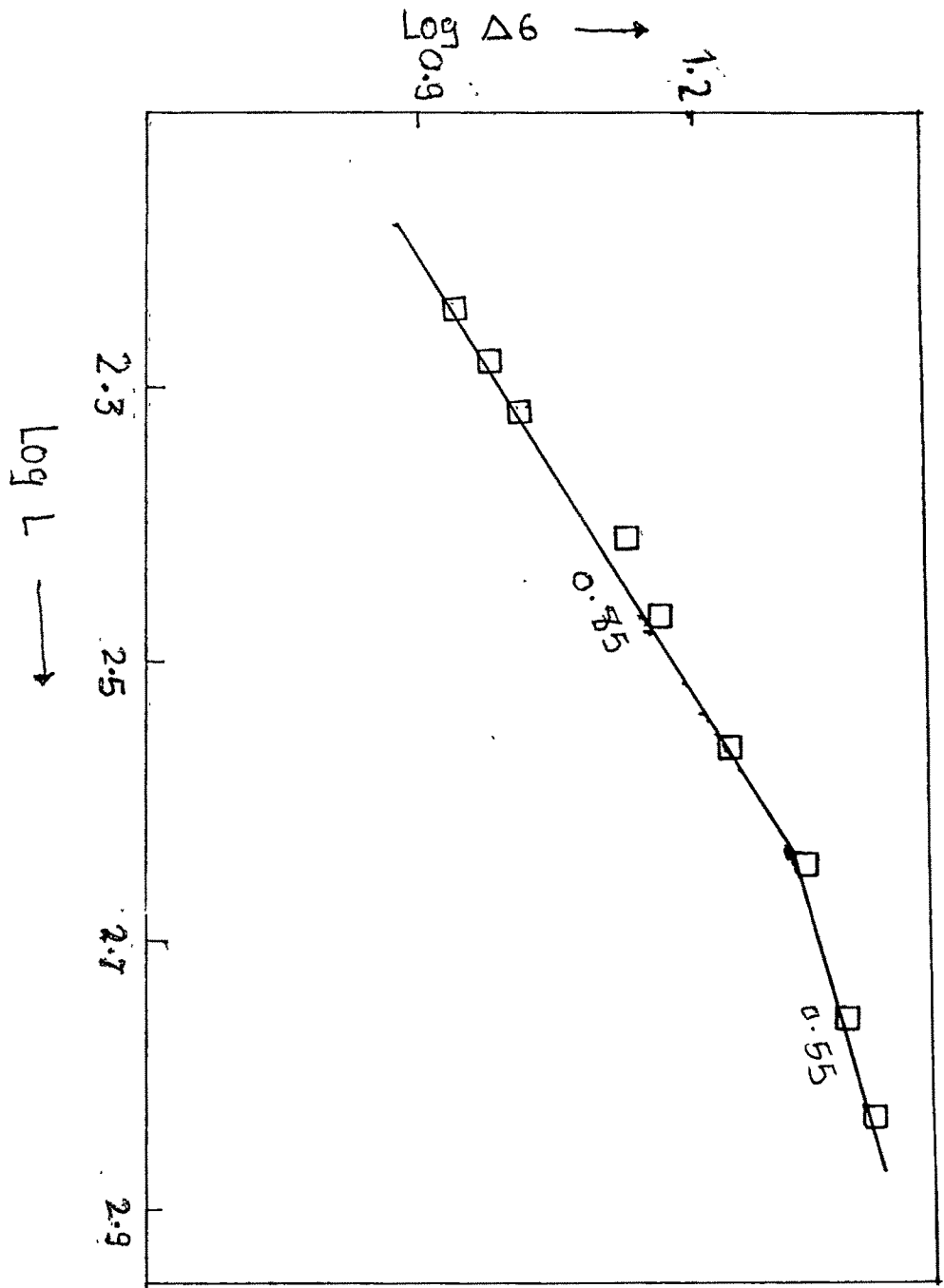


Fig. 3 [c]

the electron Fermi level in a photoconductor is raised by increasing light intensity or lowering temperature so as to include levels formally acting as electron trapping levels, the increased recombination due to these levels causes a decrease in photosensitivity^[9]. This decrease in photosensitivity manifests itself by a decrease in n , in the relation $\Delta\sigma \propto L^n$, where L is the light intensity. The decrease in photosensitivity is known to set in fairly suddenly if trapping levels involved are reasonably monoenergetic.

The excess electrons^{ca} used by illumination increase the rate of capture by the traps which are then gradually filled. The rate of filling of traps can be varied by altering the intensity of exciting light.

If an excess of electron density Δn is established by optical excitation (generation rate g_r) then

$$\Delta n = \frac{g_r}{2n_0 VS} \quad \text{-----2}$$

where n_0 is the equilibrium electron density, V is the recombination velocity and S is the cross section for recombination capture. Let us write $(n_0 VS)^{-1} = \tau$. It clearly indicates that $\Delta n \propto g_r$ if τ is a constant, or when τ changes there is substantial departure from the linear increase of photoconductivity with excitation intensity, i.e. a change in the degree of population of capture levels.

The photocurrent variations in $Sb_{0.2}Bi_{1.8}Te_3$, $Sn_{0.2}Bi_{1.8}Te_3$ and $Bi_2Te_{2.8}Se_{0.2}$

thin films with time and intensity of illumination, are shown in Figures 4 (a), (b) and (c). The sample was exposed to light for 200 seconds and then the light was extinguished and readings were taken continuously. The photoconductivity rise and decay are of considerable interest as these phenomena are sensitive to trapping effects due to impurity levels. It can be seen from Figures 4 (a), (b) and (c) that when low intensity light (242 & 344 lux) was incident on the sample, there is a steep increase in the photocurrent from A to B, followed by a slow rise from B to C and exhibiting saturation from C to D. When the light is extinguished the photocurrent suddenly decreases upto a point E and reaches a steady value beyond E. Under strong illumination (≥ 646 lux) similar rise and decay are observed except for a plateau being absent at the maximum. Since the illumination time was limited to 200 sec to avoid heating of the specimen, the saturation region was not reached in these cases.

The photocurrent during the decay will be proportional to the rate at which carriers are thermally freed from traps, multiplied by the appropriate life time for the freed carriers. Those traps which have been filled during the excitation of the material will become empty, when the excitation is removed, at a rate depending on their capture cross section and their ionization energy^[9]. If it is assumed that re-trapping of the carriers freed from traps is negligible, then an exponential decay is expected. If many different types of traps are present,

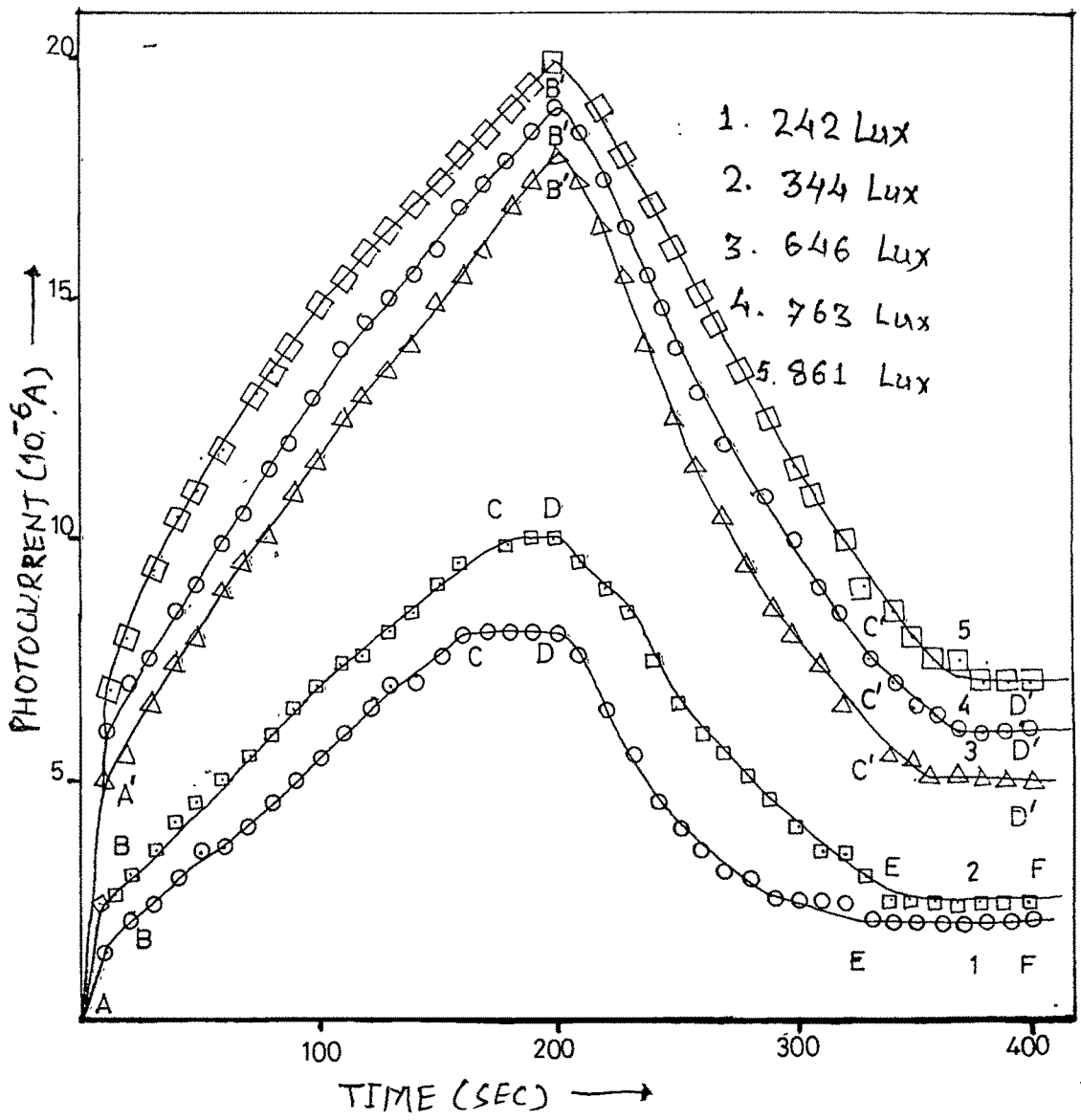


Fig. 4(a)

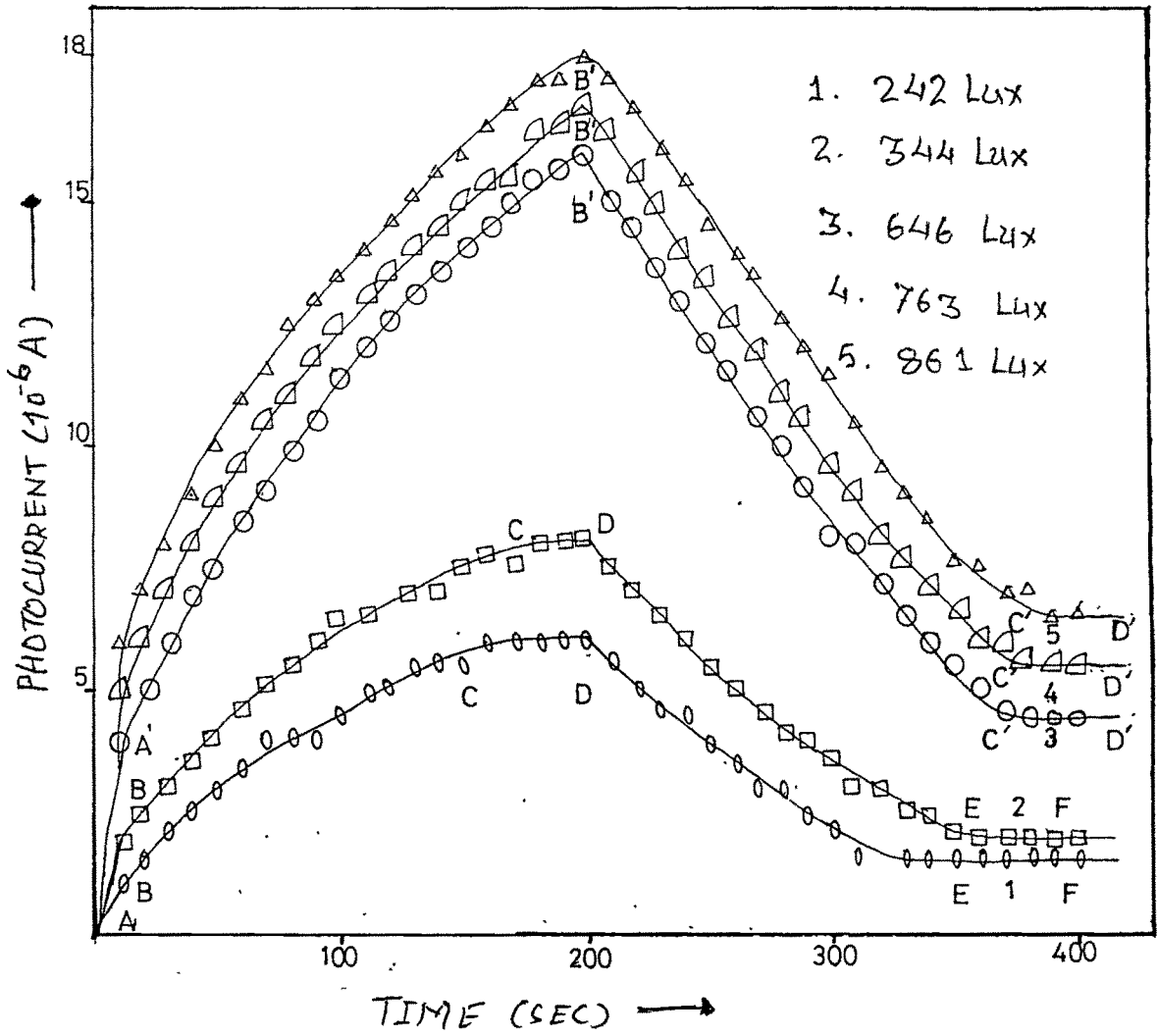


Fig. 4(b)

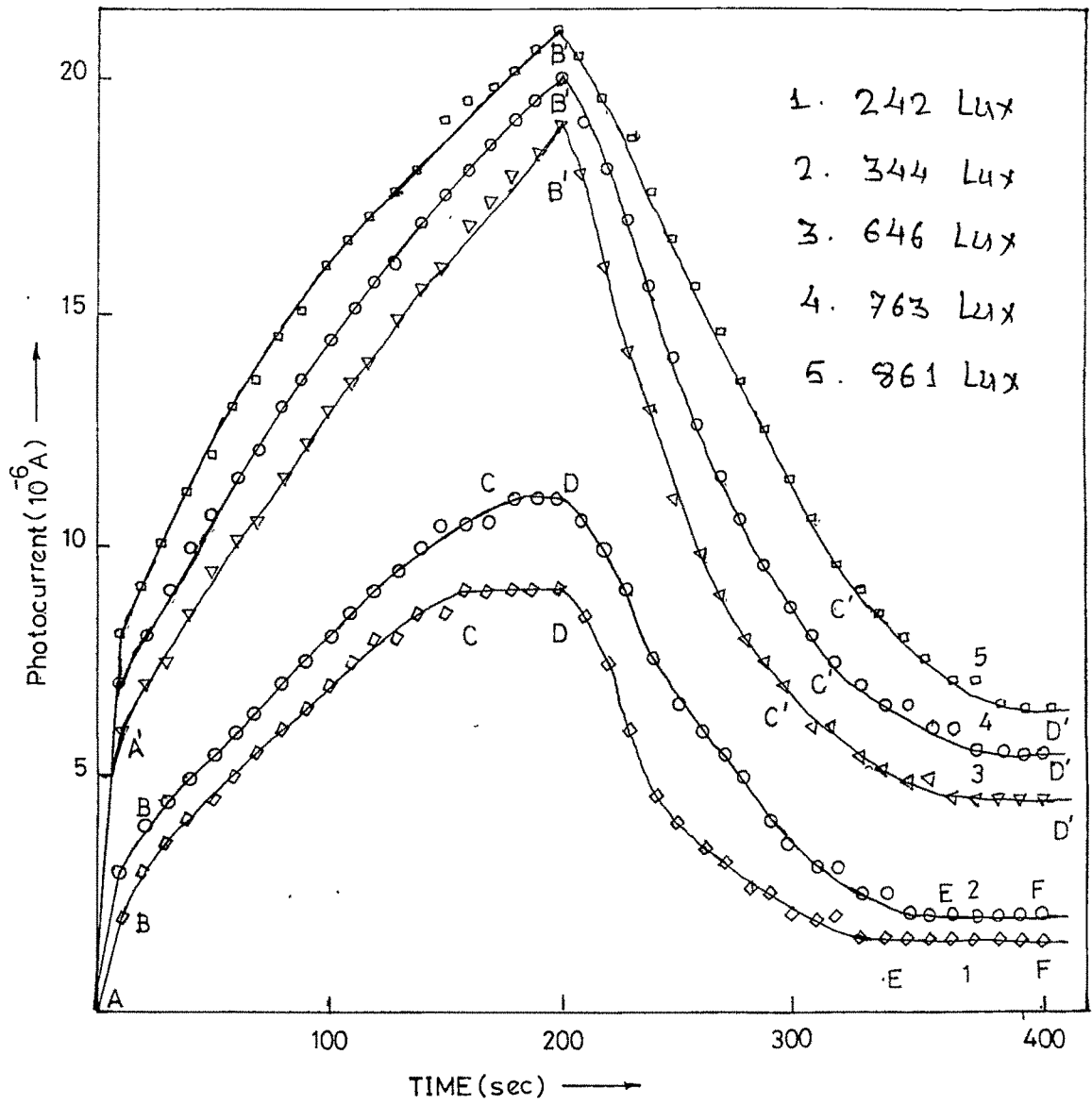


Fig. 4cc)

with different capture cross sections and ionization energies, as seems to be frequently the case, the decay curve has time dependence which can be expressed generally as

$$I = I_0 t^{-n} \quad \text{----- 3}$$

where t is the time, I_0 is the initial carrier concentration, I is the carrier concentration at time t and n is a constant which may vary in different ranges of t and also be dependent on illumination intensity. Thus the photocurrent decay should follow a similar power law. The plots of \log (photocurrent) versus \log (time) in the decay region are as shown in Figures 5 (a), (b) 6 (a),(b) and 7 (a), (b) for two extreme illumination intensities and for the three materials. The values of decay constant obtained at different illumination intensities are shown in Table-1 for these materials. There is observed a substantial decrease in n at higher intensities.

The photoconductivity rise and decay results obtained agree with those observed by Hornbeck et al. [10] in p-type silicon where the rise and decay of photoconduction was found to be due to the presence of shallow and deep traps in the material. With reference to Figure 4, the photoconductive rise from A to B is caused by excess electrons and holes produced by light in the conduction and valence bands. These photogenerated carriers reach equilibrium concentration in a time which is of the order of the life time of the electrons in the material. The

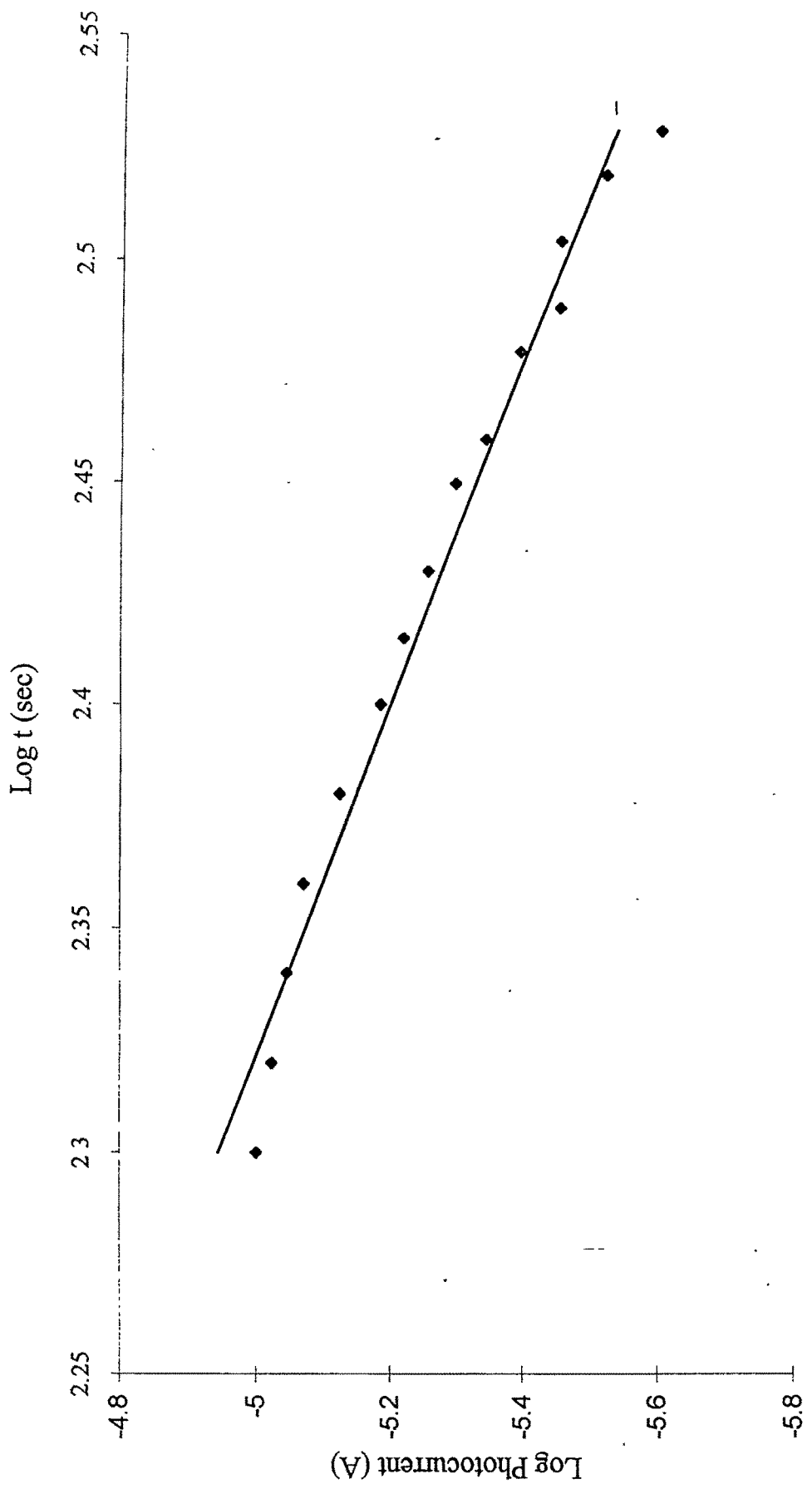


Fig. 5(a)

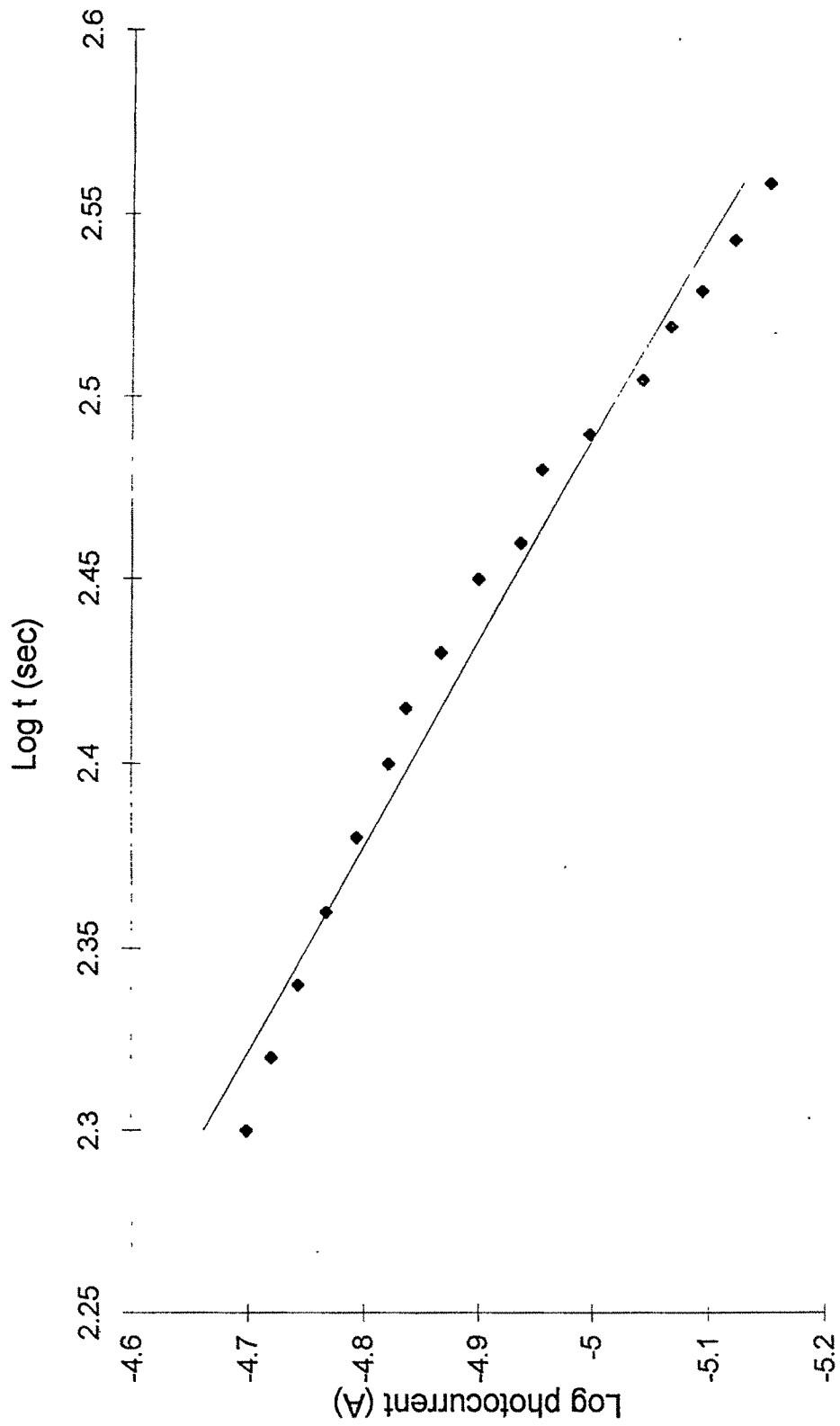


Fig. 5(b)

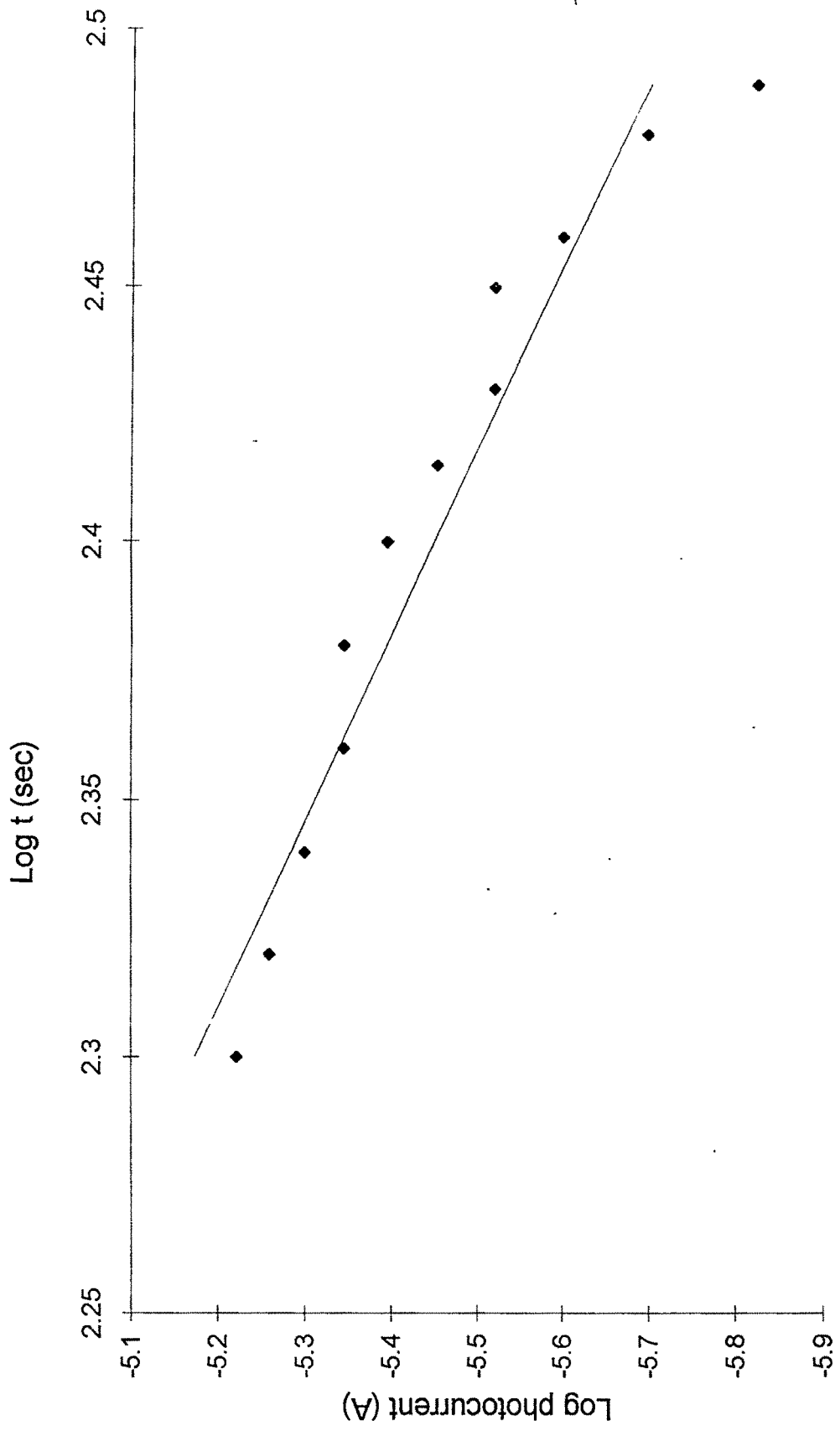


Fig. 6(a)

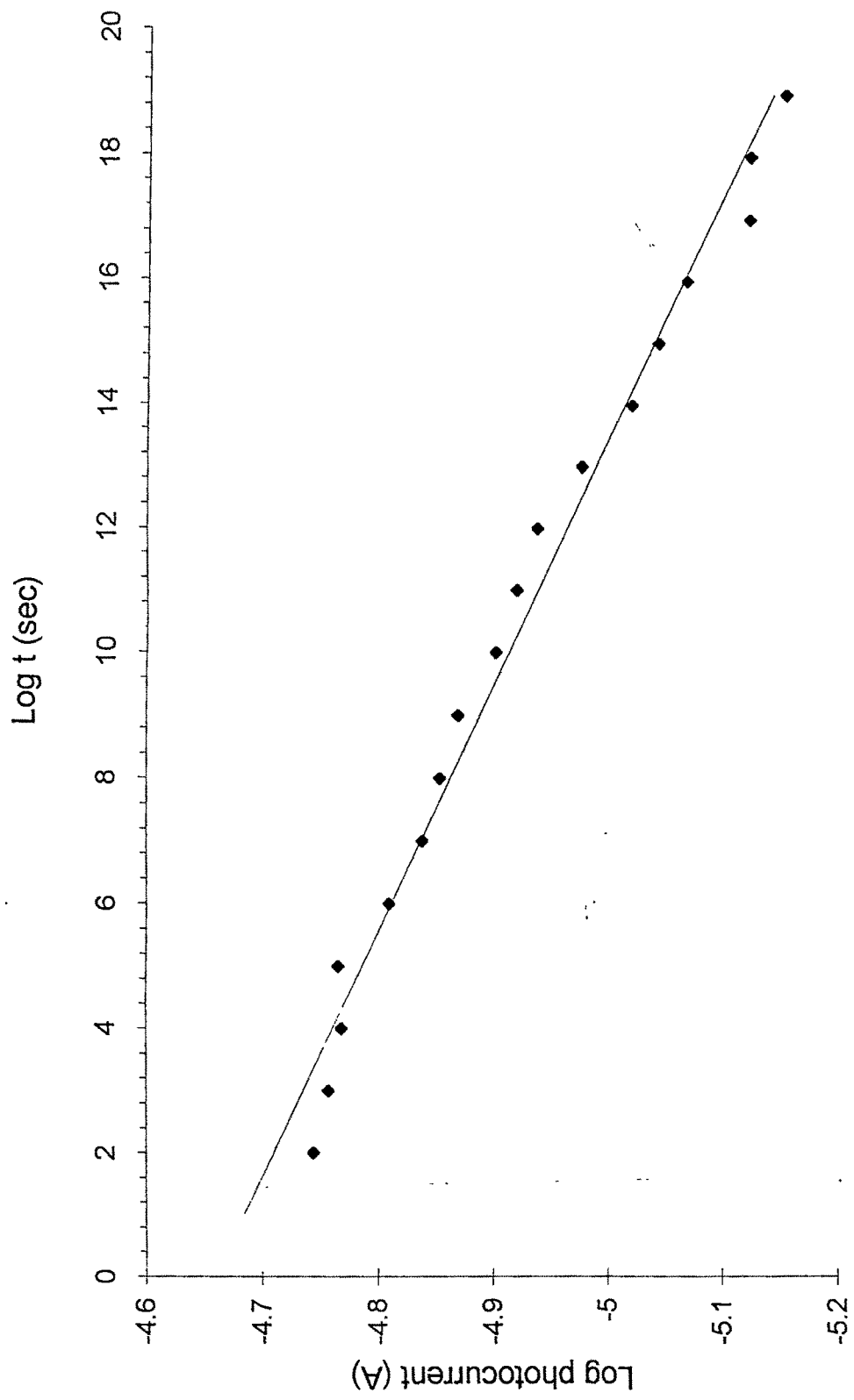
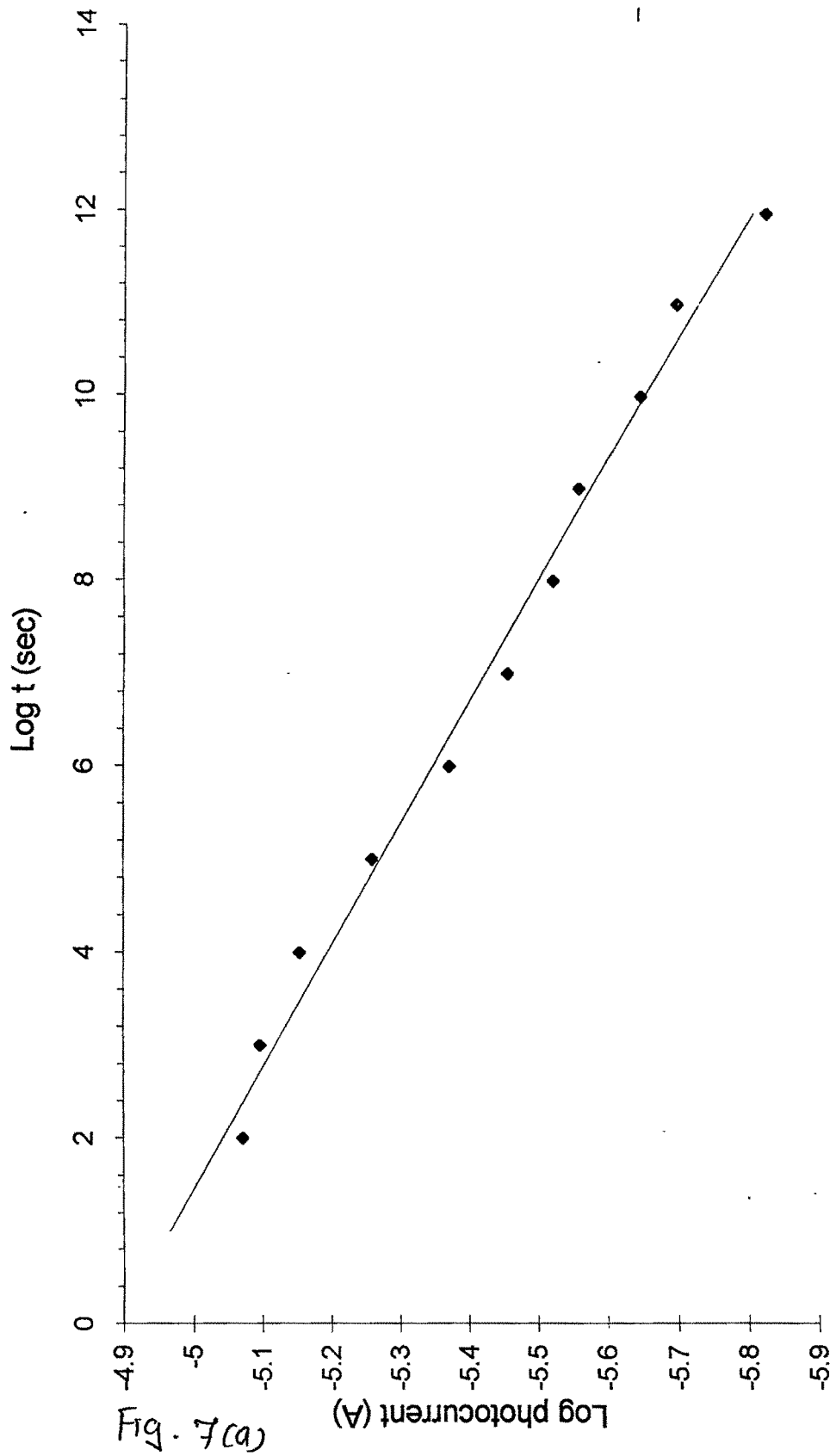


Fig. 6(b)



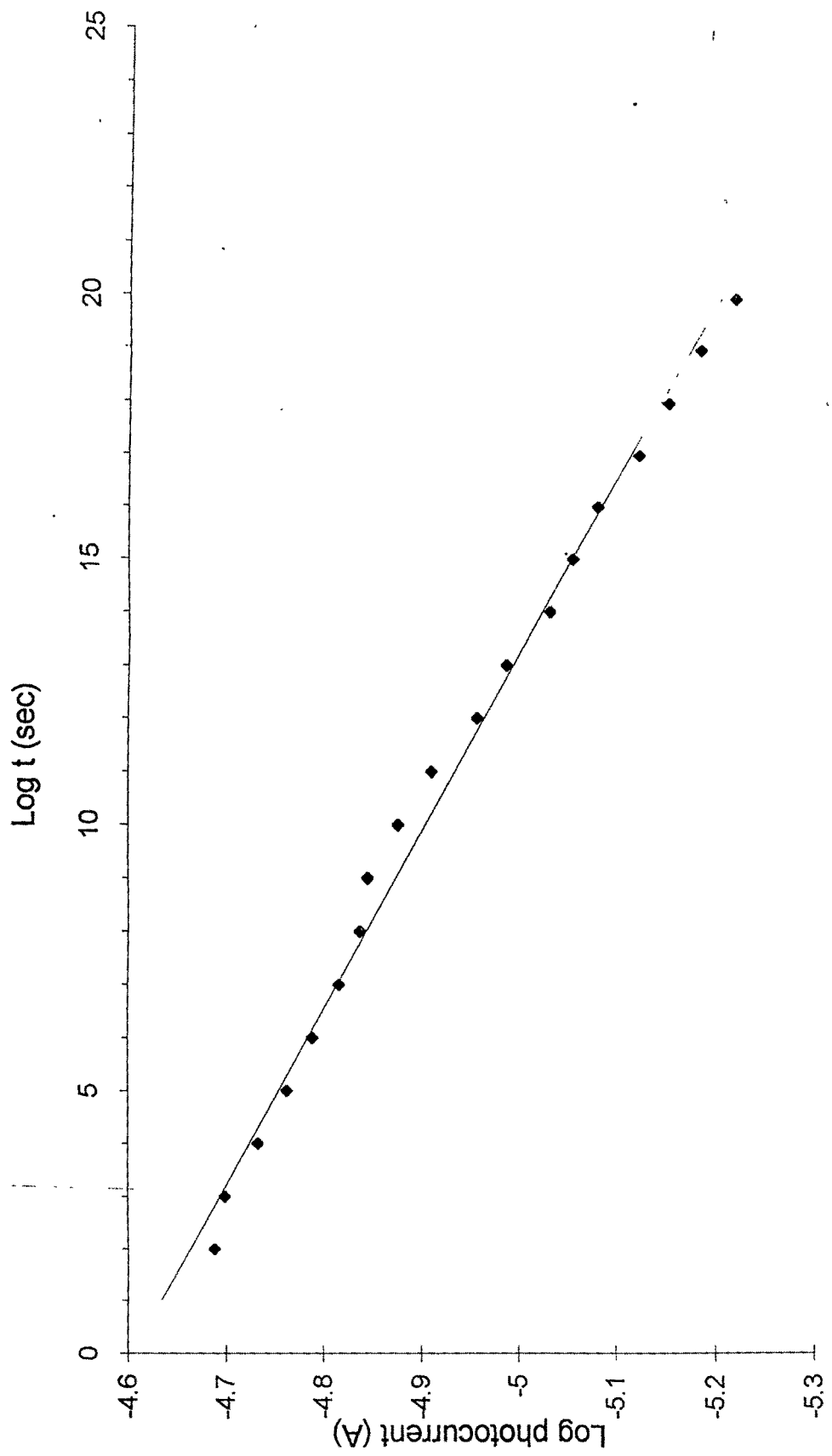


Fig. 7(b)

TABLE - 1

	Decay Constant , n		
Intensity Lux	Sb_{0.2} Bi_{1.8} Te₃	Sn_{0.2} Bi_{1.8} Te₃	Bi₂ Te_{2.8} Se_{0.2}
242	2.58	2.09	0.076
861	1.8	0.026	0.030

slow increase in photoconductivity from B to C and almost constant photoconductivity from C to D are an evidence of trapping of carriers in shallow traps. When the light is switched off, the drop in photoconductivity reflects the decrease in carrier density caused by recombination of excess electrons and holes in the conduction and valence bands, i.e., a normal recombination process. The steady photoconductivity beyond E is slightly higher than the original value which may be because of the filling of deep traps that may occur in this time scale. In a number of compound semiconductors also such behaviour has been observed. For example, similar results were obtained by Dutta et al.^[14] in the case of PbSe thin films, Bhatt et al ^[13] in the case of SnSe and Patel et al^[12] in the case of AgInSe₂ thin films.

VARIATION OF PHOTOCURRENT WITH TEMPERATURE :

The temperature of the sample under illumination was varied from room temperature to about 403K and the photocurrent was measured. The variation of photocurrent with temperature of the film under constant light intensity (646 lux) is as shown in Figure 8 (a), (b) and (c) . There is a peak at 353 K, above which the photocurrent decreases with increase in temperature of the film. This is due to the fact that, if the traps are filled by excitons at a low temperature, they may be emptied by raising the temperatre. Usually for the sake of

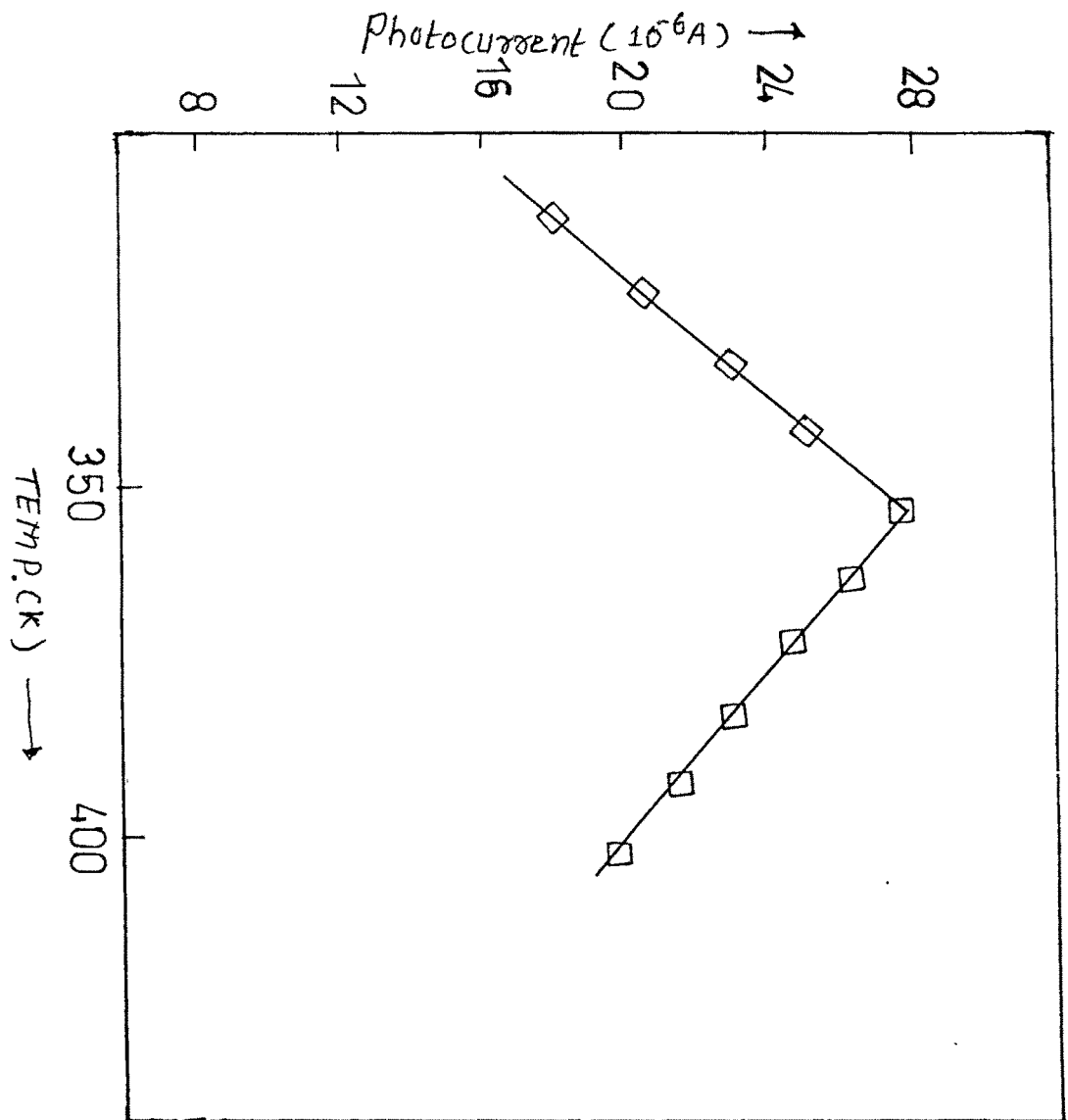


Fig. 8(a)

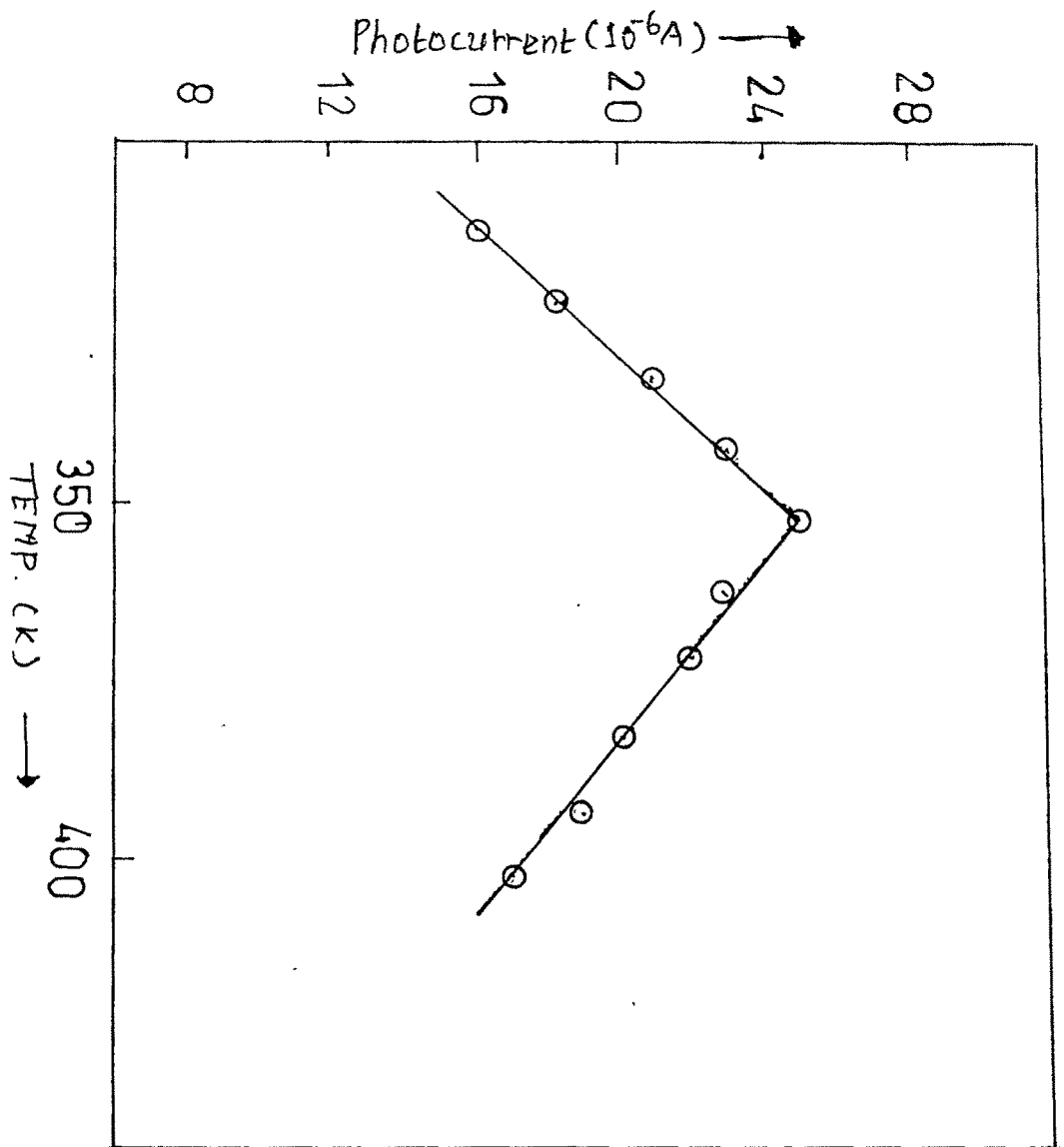


Fig. 8(b)

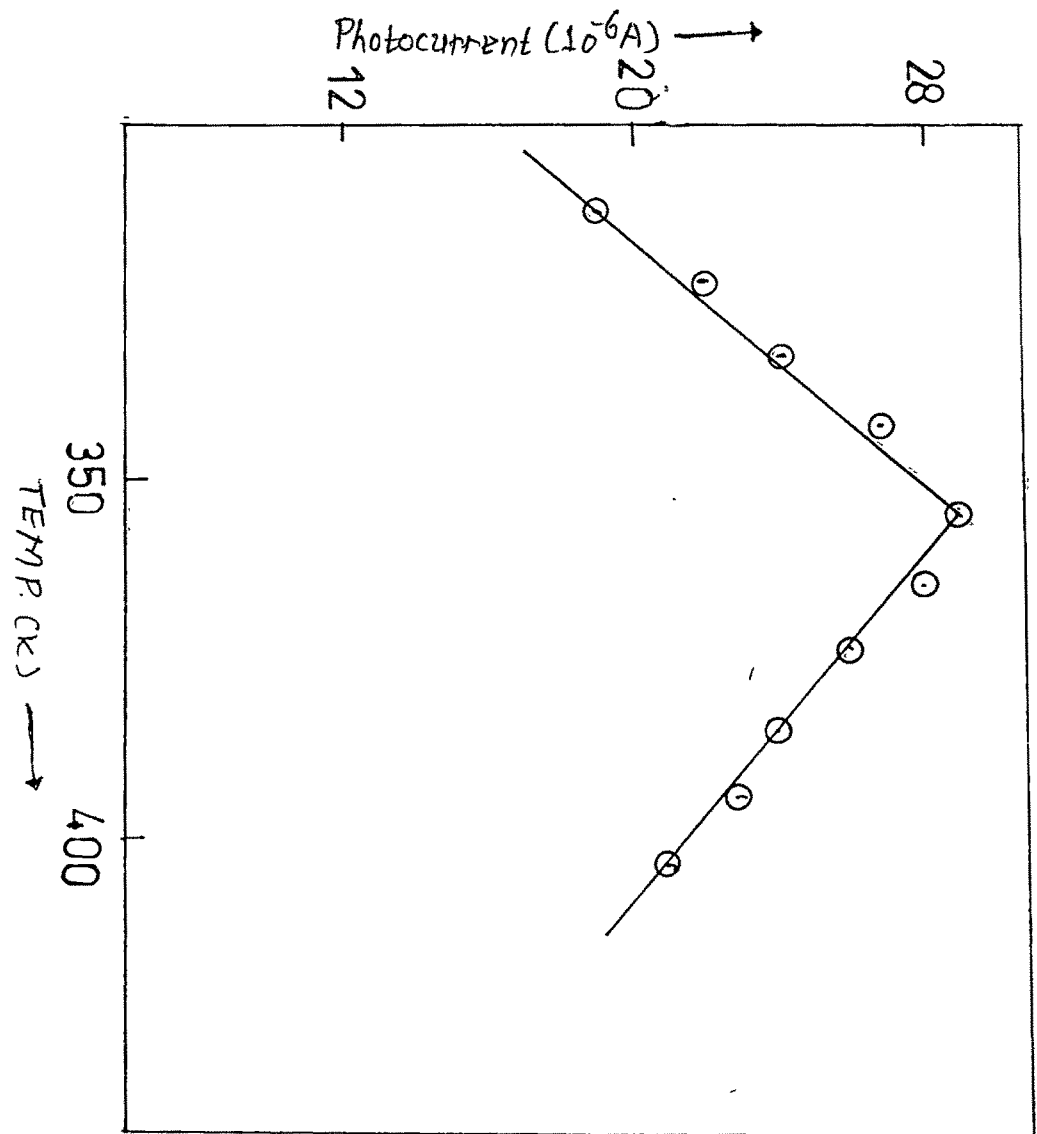


Fig. 8(c)

convenience the temperature is raised nearly at a steady rate. The increase of thermally stimulated conductivity is proportional to the rate of trap emptying multiplied by the appropriate life time. A curve of current for single trap depth is somewhat asymmetric with a fairly sharp maxima at a temperature (as in the present case), which is determined by the capture cross section of the trap and the heating rate.

Scharnhorst ^[3] explained a transition from $\Delta n/n_0 \gg 1$ (where Δn is the excess electron density and n_0 is the equilibrium electron density), at low temperature to $\Delta n/n_0 \ll 1$ at high temperature to account for the peaks observed in the photocurrent variation with temperature. According to his model, the temperature dependence of photoconductivity is through

$$\Delta\sigma(T) \propto \mu_0 n_0(T) = \mu \Delta n$$

The maxima in $\Delta\sigma(T)$ will be observed regardless of the magnitude of fixed intensity of illumination, (where n is the excess electron density, n_0 is the equilibrium electron density, μ is the carrier mobility and $\Delta\sigma$ photoconductivity), if, in addition, $\mu(T)$, the carrier mobility, is a monotonic function of T , which decreases more slowly than $n_0(T)$.

CONCLUSIONS :

1. From the plot of \log of $\Delta\sigma$ versus $\log L$ it can be concluded that $\Delta\sigma \propto L^n$, where n is around 1 up to $L = 646$ Lux and for $L > 646$ lux, n is around 0.6. This change in n can be assigned to the change in behaviour of a center from that of a trap to that of a recombination center.
2. The photoconductivity rise and decay observed in the present case show the presence of shallow traps.
3. It is also observed that the photoconductivity increases with temperature of the samples up to 353 K and then decreases. This is probably due to emptying of traps up to 353 K whereas the sharp maxima indicate the possibility of single trap depths.

REFERENCES :

1. Richard H. Bube and Alan L. fahren Bruch : Fundamental of solar cells, Academic press, New York (1983).
2. R. H. Bube : Photoconductivity of solids, John Wiley and Sons Inc. New York, London (1960).
3. K. P. Scharnhorst and H. R. Riedl : J. of Apply Phys. 43 (1972) 5142.
4. A. Rose : Phys. Rev. 97 (1955) 322.
5. H. Okimura and Y. sakai, Japan J. of Appl. Phys. 1 (1968) 731.
6. M. Buragotian and A.K.Barua, Thin solid films 99 (1983) L1.
7. B. K. Gupta, O.P.Agnihotri and Amar Raza, Thin solid films 48, (1978) 153.
8. R. Horiba, H. Nakanishi, s. Endo and T. Iric, Surface Science 86 (1979) 498.
9. V.S.Vavilov, Effects of Radiation on Semiconductors (Consultants Bureau, N.Y., 1965) p.81.
10. J. A. Hornbeck and J. R. Haynes, Phys. Rev. 97 (1955) 31.
11. S. K. Dutta, A. K. Chaudhari and H. N. Bose, Indian J. Phys. 52A (1978) 379.
12. S. M. Patel and G. Kapale, Thin Solid Films (electronics and Optics) 148 (1987) 143.
13. V. P. Bhatt, K. Gireesan and C. F. Desai, J. Mater. Sci, letters 11 (1992) 380.

Electrical Resistivity and Optical Band Gap of Doped Bi_2Te_3 Single Crystals

C.F. Desai and P.H. Soni

Physics Department, Faculty of Science,
The M S University of Baroda, Vadodara - 390 002, India

The V-VI compounds are narrow bandgap semiconductors and useful as thermoelectric device materials. Particularly Bi_2Te_3 among these is known to have high potential for thermoelectric generation. It usually has n-type conductivity and a bandgap of about 0.16 eV. There have been various studies on the bulk and thinfilm characteristics of Bi_2Te_3 , both pure and doped with Sb, including the optical and electrical properties. There is also a report on microhardness of Bi_2Te_3 single crystals. While, majority of work on this system has been aimed at thermoelectric characterization, little, if any, has been reported on the effects of dopants other than Sb. The authors report in this paper the results of their electrical resistivity and optical band gap study of single crystals of Bi_2Te_3 doped with Se, Sn, and Sb at the level of 4 atomic percentage of each. For conductivity measurements, four probe technique was used along the cleavage surfaces of the crystals. The resistivity was measured in the temperature range 35 °C to 130 °C and the temperature dependence of resistivity was used to obtain the activation energy.

The optical absorbance of these crystals was measured in the wave number range from 500 to 4000 cm^{-1} and the absorption coefficient α was calculated as a function of photon energy. The plots of $(\alpha h\nu)^2$ Vs photon energy ($h\nu$) were used to evaluate the optical band gaps. The transitions in all the cases were observed to be allowed direct type. The results are discussed in the paper.

INTRODUCTION

The V-VI group compounds are narrow band gap semiconductors and known to find applications ranging from photoconductive targets in TV cameras to I.R. spectroscopy. Among these Bi_2Te_3 is the most potential material for thermoelectronic devices (1-2). It crystallizes into a rhombohedral structure with space group $R\bar{3}m$. Its melting point is about 573 °C. It usually has n - type conductivity and a band gap of about 0.16 eV. There have been various studies on the bulk and thin film characteristics of Bi_2Te_3 , including thermoelectric characterization and optical and electrical properties (3-5). There is also a report on microhardness of Bi_2Te_3 single crystals (3). We hereby report the electrical resistivity and optical band gap of Bi_2Te_3 doped with Sb, Se and Sn at the level of 4 atomic percentage each.

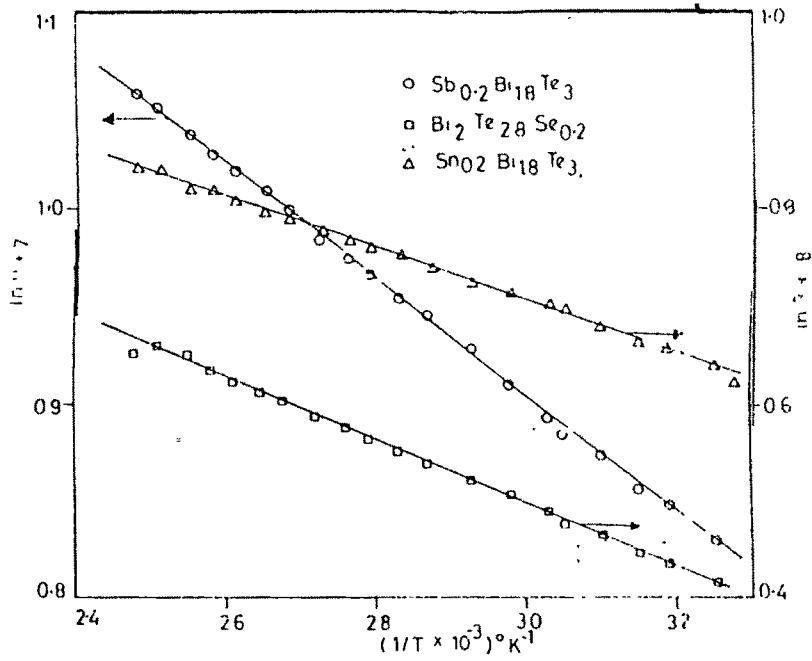


Fig. 1. Plot of $\ln S_0$ vs $1/T$

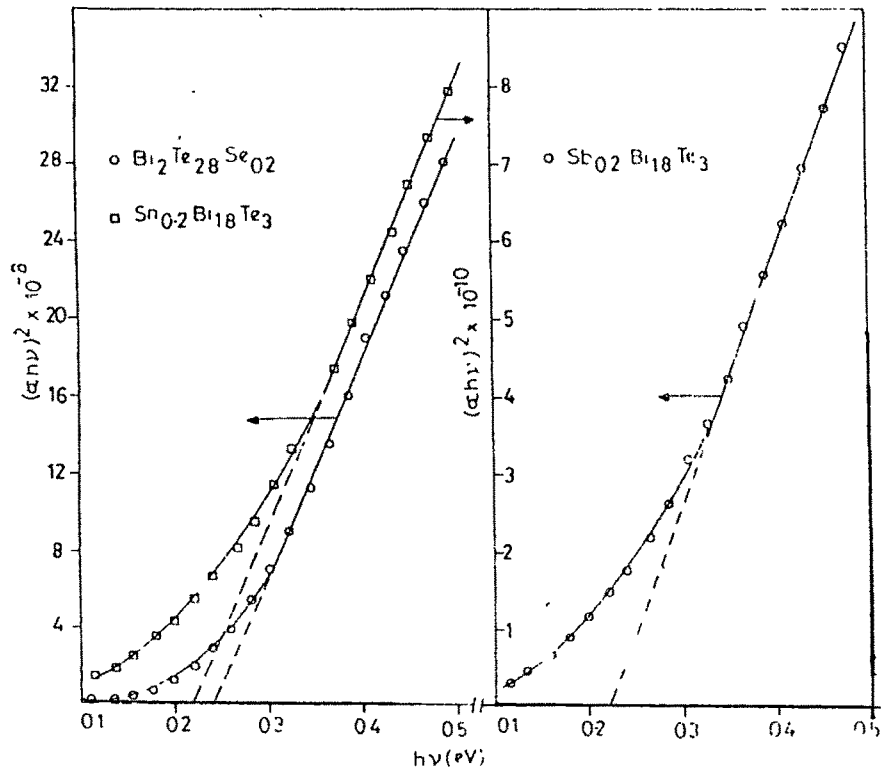


Fig. 2. Plot of $(\alpha h\nu)^2$ vs $h\nu$

EXPERIMENTAL

The single crystals were obtained from stoichiometric mixtures of the respective elements of 5N purity, using Bridgman - Stockbarger method. The crystal quality was such as to yield a fairly plane cleavage surface. The vacuum pressure used to seal the quartz ampoules containing the charge was of the order of 10^{-4} Pa and the ampoule lowering rate and the furnace temperature gradient were kept at 3.5 mm/hr & 45 °C/cm, respectively.

The conductivity type of the crystals was tested by the hot probe method. $Sb_{0.2}Bi_{1.8}Te_3$ and $Sn_{0.2}Bi_{1.8}Te_3$ exhibited p-type conductivity, whereas $Bi_2Te_{2.8}Se_{0.2}$ was found to be n-type. For electrical resistivity measurements, Valde's four-probe technique was used along the cleavage surfaces of the crystals. The measurements were carried out at different temperatures in the range from 35 °C to 130 °C.

For optical band gap study, a FTIR spectrophotometer (BOMEM, Canada) was used. The optical gaps were evaluated from the absorbance versus photon energy data. The spectra were repeated on two to three samples.

RESULTS AND DISCUSSION

The room temperature resistivity of $Sb_{0.2}Bi_{1.8}Te_3$, $Sn_{0.2}Bi_{1.8}Te_3$ and $Bi_2Te_{2.8}Se_{0.2}$ single crystals were measured to be $2.1 \times 10^{-3} \Omega \text{ cm}$, $0.64 \times 10^{-3} \Omega \text{ cm}$ and $0.51 \times 10^{-3} \Omega \text{ cm}$, respectively. The temperature dependence of the resistivity, ρ , of the three crystals is shown in Fig -1. The plots indicate extrinsic conduction in the temperature range used and obey the relation $\rho = \rho_0 \exp(-E_p/K_B T)$, where E_p is the resistivity activation energy. The activation energy values calculated from the corresponding slopes are found to be 0.01 eV, 0.010 eV and 0.012 eV, respectively. To access the intrinsic regime, measurements at still higher temperatures need be conducted.

The optical absorbance was measured in the wave number range from 500 to 4000 cm^{-1} . The $(\alpha h\nu)^2$ versus $(h\nu)$ plots of the respective semiconductors are shown in Fig - 2, where $h\nu =$ photon energy and $\alpha =$ relative absorption coefficient. It can be seen that the plot is linear in the region of strong absorption near the fundamental absorption edge. Thus, the absorption takes place through direct interband transition (6). The band gap is obtained by extrapolating the linear part to the zero of the ordinate. The optical band gaps, thus obtained are 0.22eV, 0.22eV and 0.24eV respectively, of $Sb_{0.2}Bi_{1.8}Te_3$, $Sn_{0.2}Bi_{1.8}Te_3$ and $Bi_2Te_{2.8}Se_{0.2}$.

ACKNOWLEDGEMENTS

The authors are grateful to the U.G.C., N Delhi, for the DRS research grant support and to the Higher Education Department, Government of Gujarat for awarding a research scholarship to one of them (PHS).

REFERENCES

1. L. Jansa, P. Lostak, J. Sramkova and J. Horak, J. Mater. Sci. 27 (1992) 6062.
2. H.P. Ha, Y.W. Cho, H.Y. Byun and J.D. Shim, J. Phys. Chem. Solids 55 (1994) 1233.
3. D. Arivuoli, F.D. Gnanam and P. Ramasamy, J. Mater. Sci. Letters 7 (1988) 711.
4. M.S. Rahmankhan and M. Akhtaruzzaman, Ind. J. Pure and App. Phys. 20 (1982) 656.
5. J. George and B. Pradeep, Solid State Commun. (U.S.A.) 56 (1985) 117.
6. Pankove, Optical Process in Semiconductors, Dover, Newyork 1967.

Download from fap - 19/4/99

1st Reading

1st read by: _____
2nd read by: _____
To: <u>Tejraj</u>
Fr: <u>File 4/99</u>

GROWTH AND DISLOCATION ETCHING OF $Sb_{0.2}Bi_{1.8}Te_3$ SINGLE CRYSTALS

C. F. DESAI, P. H. SONI, S. R. BHAVSAR and R. C. SHAH
*Department of Physics, Faculty of Science, The M. S. University of Baroda,
Vadodara-390 002, India*

Fr: File 4/99
22.10.98
22.10.98

Received 27 October 1998

$Sb_{0.2}Bi_{1.8}Te_3$ single crystals have been grown by the zone melting and Bridgman-Stockbarger methods. The freezing interface temperature gradients of $90^\circ\text{C}/\text{cm}$ and $45^\circ\text{C}/\text{cm}$, respectively, have been found to yield the best quality crystals obtainable at the growth rate of 0.35 cm/h . The crystals have been characterized by the powder XRD technique. The crystals growth by the zone melting method have been observed to exhibit certain typical features on their top free surfaces. A new dislocation etchant has been developed to give reproducible etch-pitting on the cleavage surface. Tests of this dislocation etchant have been carried out successfully and the etchant has been used to obtain dislocation density in the crystals.

1. Introduction

The V_2-VI_3 ($V=\text{Bi, Sb}$; $VI=\text{Se, Te}$) binary compounds and their pseudobinary solid solutions are highly anisotropic and crystallize into homologous layered structures parallel to the c axis. These are typically narrow band gap semiconductors — $E_g \sim 0.2\text{ eV}$, $\sim 0.35\text{ eV}$ and $\sim 0.16\text{ eV}$ for Sb_2Te_3 , Bi_2Se_3 and Bi_2Te_3 , respectively — and are known to find applications ranging from photoconductive targets in TV cameras to IR spectroscopy.^{1,3} There are also a few applications like in temperature control of laser diodes,³ optical recording systems⁴ and strain gauges.⁵ Among these compounds, Bi_2Te_3 is the material with the most potential for thermoelectric devices such as thermoelectric generators thermocouples, thermocoolers and IR sensors with the best figure of merit near room temperature.^{3,6-9} It also finds applications in electronic, microelectronic, optoelectronic and electromechanical devices.^{2,10} It has a rhombohedral structure with space group $R\bar{3}m$,¹¹ melting point 573°C and p type conductivity. There have been various studies of the optical and electrical properties of single crystals and thin films of Bi_2Te_3 .¹²⁻¹⁵ There is also a report on the microhardness of Bi_2Te_3 single crystals.² However, there is hardly any work reported in the literature

on the crystal growth and dislocation etching of Bi_2Te_3 -based pseudobinary crystals. This is particularly so in the case of the solid solutions, Bi_2Te_3 :Sb. Further, the impurity addition is also known to modify the band gap as has also been observed by the authors.¹⁶ The present paper reports the results obtained on the growth and dislocation etching of $Sb_{0.2}Bi_{1.8}Te_3$ single crystals.

2. Experimental

The stoichiometric weight proportions of the elemental materials of 5N purity were mixed and melted under a pressure of 10^{-5} torr in a sealed quartz ampoule. For this, the melt was continuously stirred for 24 h at 10 rpm and then air-quenched. The ingot so prepared was subjected to crystal growth by the zone melting and Bridgman-Stockbarger methods. For the zone melting method, the molten zone was set to a length of about 1.5 cm and the freezing interface gradient to about $90^\circ\text{C}/\text{cm}$ by controlling the furnace temperature within $\pm 5^\circ\text{C}$. Thirty alternate zone passes were given to the ingot to level off the dopant and other impurities. The zone travel rate used was 0.35 cm/h . The last of the zone-leveling passes was used for self-nucleated crystal growth. For the Bridgman-Stockbarger method, the

[In Press]

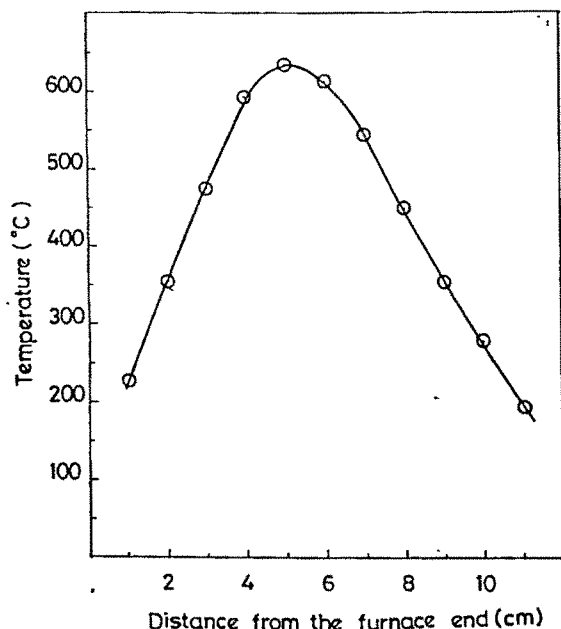


Fig. 1. Temperature profile of the zone melting furnace.

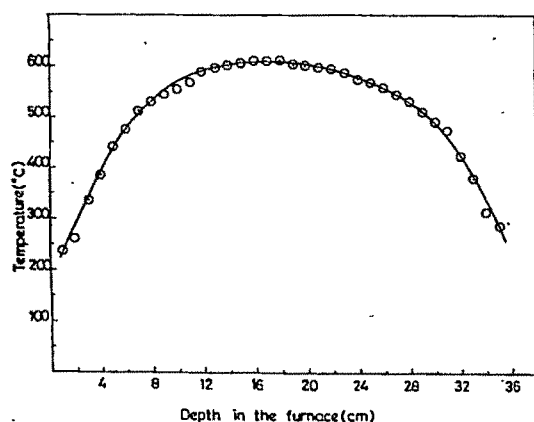


Fig. 2. Temperature profile of the Bridgman-Stockbarger furnace.

temperature gradient across the melting point at the lower end was set to $45^{\circ}\text{C}/\text{cm}$ by controlling the furnace temperature within $\pm 5^{\circ}\text{C}$. It was lowered through the gradient zone at the rate of 0.35 cm/h . Single crystals of dimension about 6 cm in length and 1 cm diameter were obtained. The temperature profiles of the zone melting and Bridgman-Stockbarger furnaces are shown in Figs. 1 and 2, respectively.

For the X-ray diffraction analysis of the powdered samples from the crystals, the X-ray diffractometer Philips PM8203 with PW1390 channel control, and the PW1373 goniometer have been used. It was operated at $35\text{--}40\text{ kV}$ and 20 mA with a Cu target ($\lambda = 1.5418\text{ \AA}$). The powdered samples from different parts of the crystal were subjected to the analysis. A new dislocation etchant capable of revealing dislocation intersecting the cleavage plane was developed using AR grade chemicals, as described below.

3. Results and Discussion

The crystals obtained by zone melting were found to exhibit some well-defined growth features on the free surface. Figures 3 and 4 show these features. Figure 3 shows layers spreading over the surface of the crystal, indicating that the layer growth mechanism is effective. Frequently, there were growth hillocks observed as shown in Fig. 4. Such hillocks with equilateral triangular sections reflect the (111) orientation of the growing crystal.

The typical X-ray powder diffraction pattern is shown in Fig. 5. The pattern consists of well-defined sharp diffraction lines. The full width at half maximum (FWHM) of the peaks confirms the good crystallinity of the specimens. The identification of the peaks in diffraction intensity was made using a JCPDS data card.¹⁷ The compound and index assignments are indicated on the major peaks in the respective plots. The observed and the JCPDS filed values are found to be in fair agreement. Bi_2Te_3 has a rhombohedral structure and its hexagonal unit cell is often used in crystal structure studies.¹¹ Y. Feutelais *et al.* have reported the values of lattice parameters

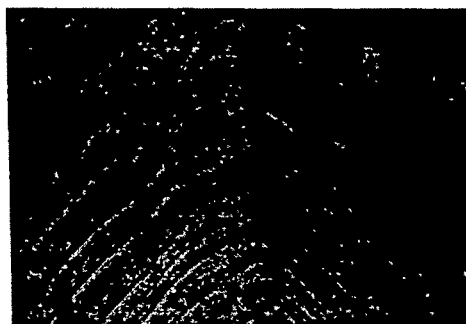


Fig. 3. Layers observed on the free surface of the as-grown crystal.

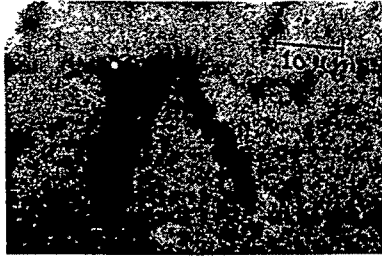


Fig. 4. Growth hillock on the crystal surface.

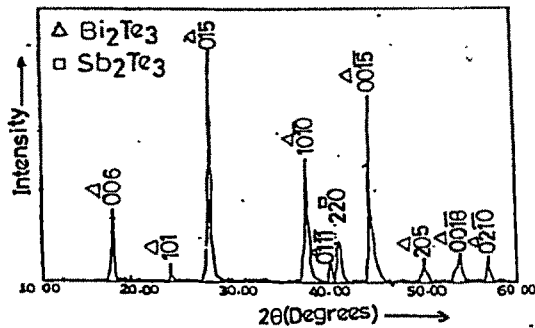


Fig. 5. XRD plot of $Sb_{0.2}Bi_{1.8}Te_3$.

of the hexagonal cell, as $a = 4.395 \text{ \AA}$ and $c = 30.44 \text{ \AA}$, in good agreement with our calculated parameters: $a = 4.387 \text{ \AA}$ and $c = 30.39 \text{ \AA}$. The crystals grown as described above were cleaved at 0°C . The constant orientation of the cleaved plane along the entire length of the ingot indicated the sample to be necessarily a single crystal. We have found no misorientation on the cleavage plane as observed under an optical microscope. This observation is supported by our etching studies. The crystals were free of grain boundaries except for occasional low angle boundaries.

A. Sagar *et al.* have reported chemical etching of Bi_2Te_3 single crystals.¹¹ Their results were found difficult to reproduce, which may be due to the presence of Sb in the present case. However, the authors, after numerous trials, have developed a dislocation etchant to work on the (111) surface of these crystals. The etchant consists of 3-part conc. solution of iodine in methanol, 0.3-part HCl (70%) and 0.3-part HNO_3 (70%). This mixture was used to etch the surface of freshly cleaved crystals. The minimum etching time to produce well-defined triangular etch



Fig. 6. Etch pit arrangement observed to delineate specific dislocation orientations.

pits at room temperature was about 30 s, and this could be extended to 60 s without deteriorating the surface to any appreciable extent. The etching was followed by rinsing the etched sample in methanol and air-drying.

The etchant produces well-defined triangular pits, exhibiting the three fold symmetry axis perpendicular to the (111) cleavage plane. Figure 6 shows the etch pattern observed after etching the specimen for 30 s. In Fig. 6, an interesting etch pit configuration is observed, *viz.* etch grooves along the [112] and [110] directions terminated by etch pits. The etch grooves produced by a dislocation etchant are known to correspond to dislocations parallel to the surface rather than inclined to it.¹⁹ Not frequently observed, such a pattern indicates a dislocation pair intersecting the observed plane and connected by dislocation lying in the surface. In the cited example, the surface-confined dislocations are along the [112] and [110] directions delineated by the etch grooves.

Etch patterns obtained on oppositely matched cleavage faces are shown in Fig. 7. There is almost one-to-one correspondence of the etch pits observed, implying that the etch pits are necessarily at dislocation sites. Figure 8 illustrates etch grooves obtained after etching the specimen for 30 s. Thus, apart from isolated dislocations, low angle boundaries are also seen to be delineated by the etch pits. Further tests for the dislocation etchant, like successive etching of a surface, scratching or indenting the surface and etching it, were conducted to obtain satisfactory results. Thus, the etchant composition stated above is capable of revealing the grown-in and freshly produced dislocations intersecting the cleavage plane.

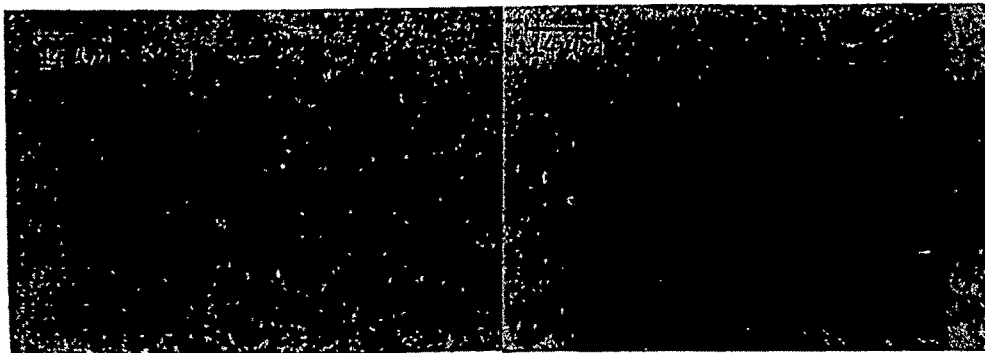


Fig. 7. Matching of etch patterns on cleavage surface counterparts.



Fig. 8. Etch grooves produced by the etchant.

The average dislocation density of the crystals grown by the Bridgman–Stockbarger and zone melting methods were found to be 1.9×10^5 and $1.4 \times 10^5 \text{ cm}^{-2}$, respectively, as measured by the etch pit count method.

4. Conclusions

The above results show that good quality single crystals can be obtained by the zone melting and Bridgman–Stockbarger methods. The observation on growth features indicates the layer mechanism to be effective in the growth of the crystal. Also, the new etchant is capable of revealing dislocation intersecting the cleavage plane.

Acknowledgment

The authors are grateful to the UGC, New Delhi, for the research grant support and to the Higher Education Department, Government of Gujarat, for awarding the research scholarship to P. H. S.

References

1. M. Stolzer, M. Stordeur, H. Sobotta and V. Rieve, *Phys. Status Solidi B* **138**, 259 (1986).
2. D. Arivuoli, F. D. Gnanam and P. Ramasamy, *J. Mater. Sci. Lett.* **7**, 711 (1988).
3. D. M. Rowe and C. M. Bhandari, *Modern Thermoelectronics* (Holt, Rinehart and Winston, London, 1981), 103.
4. K. Watanabe, N. Sato and Miyaoka, *J. Appl. Phys.* **54**, 1256 (1983).
5. Sh. B. Atakulov, T. Azimov and A. N. Shamsiddinov, *Sov. Phys. Semicond.* **16**, 1326 (1982).
6. C. H. L. Goodman, *Mater. Res. Bull.* **20**, 237 (1985).
7. L. Jansa, P. Lostak, J. Sramkova and J. Horak, *J. Mater. Sci.* **27**, 6062 (1992).
8. B. Roy, B. R. Chakraborty, R. Bhattacharya and A. K. Dutta, *Solid State Commun.* **25**, 937 (1978).
9. H. W. Jeon, H. P. Ha, D. B. Hyun and J. D. Shim, *J. Phys. Chem. Solids* **52**, 579 (1981).
10. N. Sakai, N. Kajiwara, T. Takemura, S. Minomura and Y. Fuji, *Solid State Commun.* **40**, 1045 (1981).
11. A. Sagar Jr. and J. W. Faust, *J. Appl. Phys.* **38**, 482 (1967).
12. J. George and B. Pradeep, *Solid State Commun.* **56**, 117 (1985).
13. M. S. Rahman Khan and M. Akhtaruzzaman, *Ind. J. Pure Appl. Phys.* **20**, 656 (1982).
14. L. R. Testardi and E. Burstein, *Phys. Rev. B* **6**, 460 (1972).
15. S. R. Guha Thakurta and A. K. Bose, *Ind. J. Phys.* **44**, 601 (1970).
16. C. F. Desai and P. H. Soni, *Physics of Semiconductor Devices*, eds. V. Kumar and S. K. Agarwal, **2**, 1174 (1998).
17. JCPDS (File) pub: International Center for Diffraction Data, Pennsylvania-19081, U.S.A., ed. 1982
18. Y. Feutelais, B. Legendre and N. Rodier, *Mater. Res. Bull. (U.S.A.)* **28**, 391 (1993).
19. V. P. Bhatt and G. R. Pandya, *J. Crystal. Growth* **19**, 213 (1973).

Creep activation energy of flow process in $\text{Bi}_2\text{Te}_{2.8}\text{Se}_{0.2}$ single crystals

C F DESAI, P H SONI* and S R BHAVSAR

Department of Physics, Faculty of Science, MS University of Baroda, Vadodara 390 002, India

MS received 15 October 1998

Abstract. Temperature dependence of the Vickers microhardness of $\text{Bi}_2\text{Te}_{2.8}\text{Se}_{0.2}$ single crystals has been studied. Loading time dependence of microhardness at different temperatures has been used for creep study in the temperature range 303 K–373 K. The activation energy for indentation creep of the crystals has been evaluated.

Keywords. Vickers microhardness; cleavage surface; creep; activation energy.

1. Introduction

The $\text{V}_2\text{-VI}_3$ ($\text{V} = \text{Bi, Sb}$; $\text{VI} = \text{Se, Te}$) binary compounds and their pseudobinary solid solutions are highly anisotropic and crystallize into homologous layered structures parallel to the c -axis and known to find applications ranging from photoconductive targets in TV cameras to IR detectors (Stolzerm *et al* 1986; Arivuoli *et al* 1988). $\text{V}_2\text{-VI}_3$ compounds are narrow band gap semiconductors: $E_g \sim 0.2$ eV, ~ 0.35 eV and ~ 0.16 eV for Sb_2Te_3 , Bi_2Se_3 and Bi_2Te_3 , respectively. There are also a few applications for temperature control of laser diodes (Rowe and Bhandari 1981), optical recording system (Watanabe *et al* 1983) and strain gauges (Atakulov *et al* 1982). Among these, Bi_2Te_3 is the most potential material for thermoelectric devices such as thermoelectric generators, thermocouples, thermocoolers and IR sensors with the best figure of merit near room temperature (Roy *et al* 1978; Teon *et al* 1981; Rowe and Bhandari 1981; Goodman 1985; Jansa *et al* 1992). It also finds widespread application in electronic, microelectronic, optoelectronic and electromechanical devices (Sakai *et al* 1981; Arivuoli *et al* 1988). It crystallizes into a rhombohedral structure with space group $R\bar{3}m$ (Sagar and Faust 1967). Its melting point is 573°C and has p -type semiconductivity. There have been various studies on optical and electrical properties of single crystals and thin films of Bi_2Te_3 (Guha Thakurta and Bose 1970; Testardi and Burstein 1972; Rahman Khan and Akhtaruzzaman 1982; George and Pradeep 1985). There is also a report on microhardness of Bi_2Te_3 single crystals (Arivuoli *et al* 1988). However, there is hardly any work reported in literature on the microhardness of Bi_2Te_3 based pseudobinary crystals. This is particularly so in the case of solid solution, $\text{Bi}_2\text{Te}_3 : \text{Se}$. Microhardness is a general macroprobe for assessing the bond strength, apart from being

a measure of the bulk strength. Further, the impurity addition is also known to modify band gap as has been observed by the authors (Desai and Soni 1998). The present paper reports the results of investigation of the microhardness of $\text{Sb}_{0.2}\text{Bi}_{1.8}\text{Te}_3$, $\text{Sn}_{0.2}\text{Bi}_{1.8}\text{Te}_3$ and $\text{Bi}_2\text{Te}_{2.8}\text{Se}_{0.2}$ single crystals and indentation creep of the cleavage surfaces of these crystals.

2. Experimental

The single crystals were obtained from stoichiometric mixture of the respective elements of 5 N purity, using Bridgman–Stockbarger method. The crystal quality was such that it yielded a fairly plane cleavage surface. The vacuum pressure used to seal the quartz ampoules containing the charge was of the order of 10^{-4} Pa, the temperature gradient across the melting point at the lower end was set to $45^\circ\text{C}/\text{cm}$ by controlling the furnace temperature within $\pm 5^\circ\text{C}$. It was lowered through the gradient zone at the rate of 0.35 cm/h.

The hardness indentations were carried out on freshly cleaved surfaces of samples of at least 2 mm thick, using Vickers diamond pyramidal hardness tester. The indentation diagonals were measured to an accuracy of 0.19 μm using a micrometer eye piece. For the study of load dependence of hardness, the applied load was varied in the range from about 10 mN to 1000 mN. The hardness was calculated using the standard formula

$$H_v = \frac{1854p}{d^2} \times 9.8065,$$

where p is the applied load in mN obtained as the product of the load in g and g the 9.81 ms^{-2} , d the average of the two indentation mark diagonal lengths in μm and H_v the Vickers hardness in MPa.

Since this equipment does not provide for high temperature hardness testing, a simple hot stage was prepared

*Author for correspondence

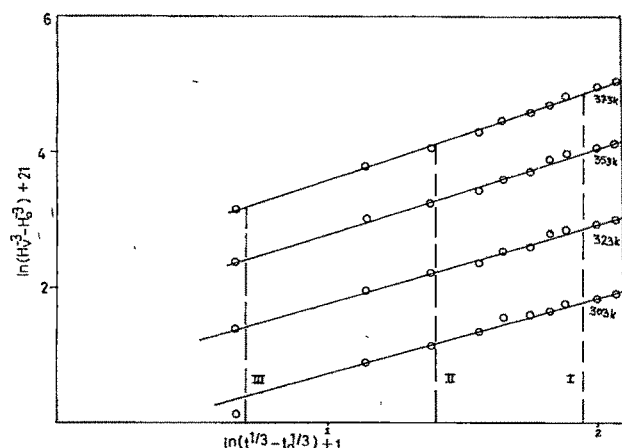


Figure 3. Plots of $\ln(H_v^{-3} - H_{v0}^{-3}) + 21$ vs $\ln(t^{1/3} - t_0^{1/3}) + 1$

three sets of $\ln(H_v^{-3} - H_{v0}^{-3})$ values at different temperatures were obtained for three different values of $\ln(t^{1/3} - t_0^{1/3})$ indicated by vertical broken lines. These values of $\ln(H_v^{-3} - H_{v0}^{-3})$ were plotted against the inverse of corresponding temperature (figure 4). Again these curves are straight lines with approximately equal slopes according to (2). The slope represents the value of $-Q/3R$. The energy value obtained in the present case, 117 kJ/mol, is similar to those at low homologous temperatures in the cases like Ag, Cu, Ni, Co etc. A dislocation pipe diffusion mechanism may explain this.

Acknowledgements

The authors are grateful to the UGC, New Delhi, for the research grant support and to the Higher Education Department, Government of Gujarat for awarding the research scholarship to one of the authors (PHS).

References

- Arivuoli D, Gnanam F D and Ramasamy P 1988 *J. Mater. Sci. Lett.* **7** 711
 Atakulov Sh B, Azimov T and Shamsiddinov A N 1982 *Sov Phys. Semicond.* **16** 1326
 Atkins A G 1973 *The science of hardness testing and its research application* (eds) J H Westbrook and H Conrad (Ohio: ASM) Ch. 17
 Atkins A G, Silverio A and Tabor D 1966 *J. Inst. Metals* **94** 369

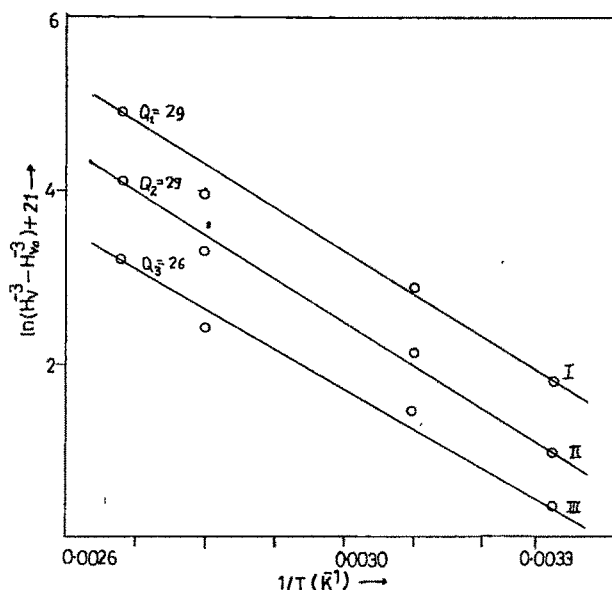


Figure 4. Plots of $\ln(H_v^{-3} - H_{v0}^{-3}) + 21$ vs $1/T$.

- Bhatt V P and Desai C F 1982 *Bull. Mater. Sci.* **4** 23
 Desai C F and Soni P H 1998 *Physics of semiconductor devices* (eds) V Kumar and S K Agarwal (Delhi: Narosa) **2** p. 1174
 George J and Pradeep B 1985 *Solid State Commun.* **56** 117
 Goodman C H L 1985 *Mater. Res. Bull.* **20** 237
 Guha Thakurta S R and Bose A K 1970 *Indian J. Phys.* **44** 601
 Jani T M, Pandya G R and Desai C F 1995 *Cryst. Res. Technol.* **30** K17
 Jansa L, Lostak P, Sramkova J and Horak J 1992 *J. Mater. Sci.* **27** 6062
 Jeon H W, Ha H P, Hyun D B and Shim J D 1981 *J. Phys. Chem. Solids* **52** 579
 Rahman Khan M S and Akhtaruzzaman M 1982 *Indian J. Pure & Appl. Phys.* **20** 656
 Rowe D M and Bhandari C M 1981 *Modern thermoelectronics* (London: Holt, Rinehart and Winston) p. 103
 Roy B, Chakraborty B R, Bhattacharya R and Dutta A K 1978 *Solid State Commun.* **25** 937
 Sagar A and Faust Jr J W 1967 *J. Appl. Phys.* **38** 482
 Sakai N, Kajiwara N, Takemura T, Minomura S and Fujii Y 1981 *Solid State Commun.* **40** 1045
 Stolzerm M, Stordeur M, Sobotta H and Riede V 1986 *Phys. Status Solidi B* **138** 259
 Testardi L R and Burstein E 1972 *Phys. Rev.* **B6** 460
 Watanabe K, Sato N and Miyaoka S 1983 *J. Appl. Phys.* **54** 1256

Microhardness of Sb-, Sn- and Se-doped Bi₂Te₃ single crystals

C F Desai, P H Soni & S R Bhavsar

Physics Department, Faculty of Science, M S University of Baroda, Vadodara 390 002

Received 4 September 1998, 26 November 1998; accepted 1 February 1999

The Vickers microhardness indentations have been carried out on the cleavage faces of Sb_{0.2}Bi_{1.8}Te₃, Sn_{0.2}Bi_{1.8}Te₃ and Bi₂Te_{2.8}Se_{0.2} single crystals obtained by Bridgman-Stockbarger method. The applied load dependence and surface anisotropic variations of hardness have been studied. All the three crystals exhibit impurity hardening to an extent of 30-45% compared to the pure Bi₂Te₃ crystal, whereas, a maximum hardness anisotropy, to an extent of 20%, is exhibited by the Sn doped crystals. Detailed results have been reported.

1 Introduction

The V₂-VI₃ (V-Bi, Sb, VI-Se, Te) binary compounds and their pseudobinary solid solutions are highly anisotropic and crystallize into homologous layered structures parallel to the *c*-axis and known to find applications ranging from photoconductive targets in TV cameras to IR Spectroscopy.¹⁻² V₂-VI₃ compounds are narrow band gap semiconductors: $E_g \sim 0.2\text{eV}$, $\sim 0.35\text{eV}$ and $\sim 0.16\text{eV}$ for Sb₂Te₃, Bi₂Se₃ and Bi₂Te₃, respectively. There are also a few applications for temperature control of laser diodes³, optical recording system⁴ and strain gauges⁵. Among these, Bi₂Te₃ is the most potential material for thermoelectric devices such as thermoelectric generators, thermocouples, thermocoolers and IR sensors with the best figure of merit near room temperature^{3,6-9}. Bi₂Te₃ finds applications in electronic, microelectronic, optoelectronic and electromechanical devices^{2,10}. It crystallizes into a rhombohedral structure with space group R3m (Ref. 11). Its melting point is 573°C and is a p-type semiconductor. There have been various studies on optical and electrical properties of single crystals and thin films of Bi₂Te₃ (Refs 12-15). There is also a report on microhardness of Bi₂Te₃ single crystals². However, there is hardly any work on microhardness, reported in literature, on the Sb, Sn and Se doped Bi₂Te₃ single crystals. Microhardness is a general macroprobe for assessing the bond strength, apart from being a measure of the bulk strength. Further, the impurity addition is also known to modify band gap as has also been observed by the authors¹⁶. The present paper reports the results of the authors' investigation of the microhardness of Sb_{0.2}Bi_{1.8}Te₃, Sn_{0.2}Bi_{1.8}Te₃ and Bi₂Te_{2.8}Se_{0.2} single crystals.

The microhardness was measured as a function of applied load and orientation on the cleavage surfaces of these crystals.

2 Experimental Details

The single crystals were obtained from stoichiometric mixtures of the respective elements of 5N purity, using Bridgman-Stockbarger method. The crystal quality was such as to yield a fairly plane cleavage surface. The vacuum pressure used to seal the quartz ampoules containing the charge was of the order of 10^{-4}Pa and the ampoule lowering rate and the furnace gradient were kept at 3.5 mm/hr and 45°/cm, respectively.

The hardness indentations were carried out on freshly cleaved surfaces of samples at least 2mm thick, using Vickers diamond pyramidal hardness tester. The indentation diagonals were measured to an accuracy of 0.1 μm using a micrometer eye piece. For the study of load dependence of hardness, the applied load was varied in the range 10 to 1000 mN. For the study of surface anisotropy of hardness, the azimuthal orientation of the crystal surface was varied from 0 to 90° with reference to a fixed direction in the surface, keeping the applied load constant. The indentation time was kept constant at 20 s in all the cases. The hardness was calculated using the standard formula:

$$H_v = \frac{1854 p}{d^2}$$

where p = applied load in mN obtained as the product of the load in gm and $g = 9.81\text{ms}^{-2}$, d = average of the two indentation mark diagonal lengths in μm and H_v = Vickers hardness in MPa.

The results, discussed below, are based on the observations averaged over at least three indentations produced at each variable value and a particular indentation set repeated on two to three samples

3 Results and Discussion

Fig 1 gives the plots of the Vickers hardness (H_v) versus applied load (p), obtained for the Sb, Sn and Se doped crystals

The complexity observed in the load dependence of hardness closely parallels many reports on a variety of crystals¹⁷⁻¹⁹ Particularly, the low load range (i.e. 200 mN or less) defies the Kick's Law²⁰ which implies hardness to be independent of load This dependence is normally ascribed to the strain hardening of the surface layers responding to the progressive penetration of the loaded indenter²¹⁻²² The hardness peaks are in turn explained in terms of the resulting deformation-induced coherent regions. Beyond a certain depth of penetration, which corresponds to the expanse of the coherent region and to the load at the peak hardness, the indenter penetrates the virgin layers which easily favour nucleation and multiplication of dislocations²²⁻²³ It is observed (Fig 1) that the hardness is independent of load for loads beyond 300 mN and represents the true hardness of the bulk of the crystal Accordingly, the hardness values of $Sb_{0.2}Bi_{1.8}Te_3$, $Sn_{0.2}Bi_{1.8}Te_3$ and $Bi_2Te_{2.8}Se_{0.2}$ crystals are

630, 642 and 582 MPa respectively (Fig 1). The reported value of the pure Bi_2Te_3 crystal is about 448 Mpa^2 . Thus there is a significant impurity hardening observed with all the three dopants, the maximum, ~45%, being that due to Sn doping The plots of $\ln p$ versus $\ln d$ (where d = indentation diagonal length), follows the Meyer's law²⁴, $p = ad^n$ with different values of n in different load ranges (Fig. 2) It is observed to be nearer to 2 in the high load range, reflecting the hardness saturation in this load range. Whereas, the Meyer indices in the low load ranges for the three crystals are calculated to be 2.83, 4.82 and 3.28, respectively, in the cases of Sb, Sn and Se doped crystals. These values far-exceed the ideal value 2 indicating high work hardening capacities of the crystals

The surface anisotropic variations of H_v in the three cases are represented in Fig 3. The plots show a periodicity corresponding to the 12-fold symmetry about the loading axis which, in the present case, is normal to the cleavage plane (III). This is a result of the 3-fold symmetry of the crystals combined with the 4-fold symmetry of the indenter. It can be seen that there is maximum anisotropy (of about 20%) in the case of the Sn doped crystals

4 Conclusion

The hardness values of $Sb_{0.2}Bi_{1.8}Te_3$, $Sn_{0.2}Bi_{1.8}Te_3$ and $Bi_2Te_{2.8}Se_{0.2}$ single crystals have been obtained to be

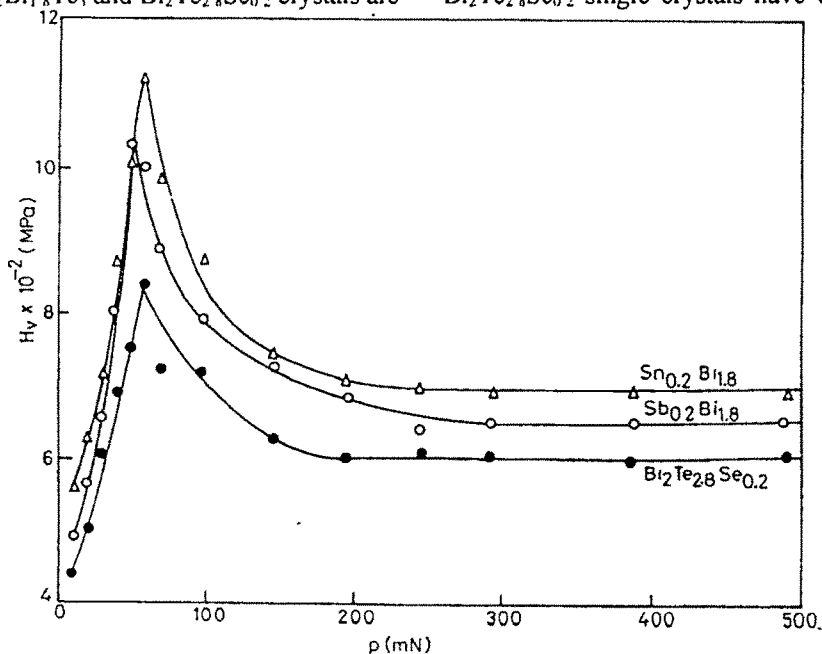
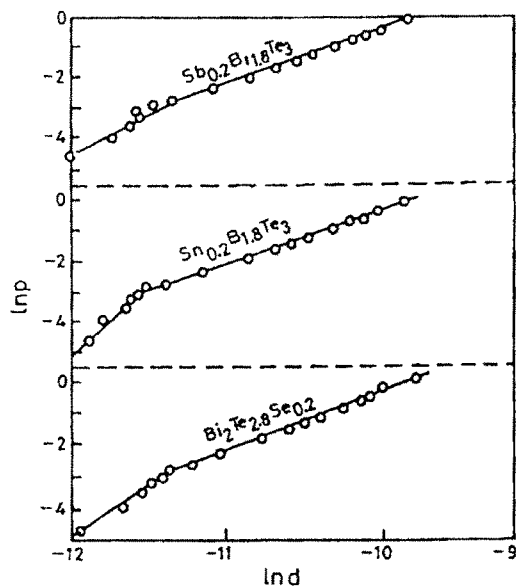
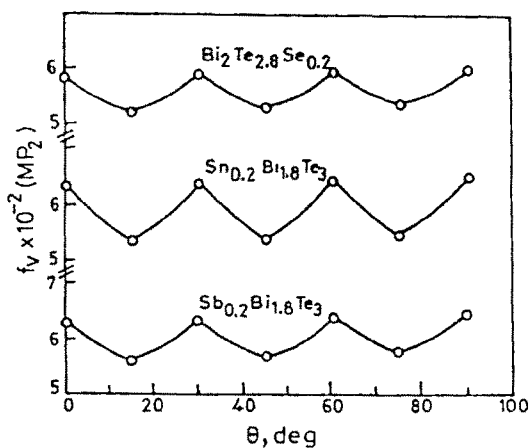


Fig 1 — Plots of H_v versus p

Fig 2 — Plots of $\ln p$ versus $\ln d$ Fig 3 — Plots of H_v versus orientation angle θ

630, 642 and 582 MPa, respectively, which are significantly higher than the reported hardness of the pure Bi_2Te_3 crystals. The work hardening capacity of Sn doped crystals has been observed to be the highest among the three crystals. The surface anisotropic variations of hardness are observed to be maximum (~20%) in the case of Sn doped crystals.

Acknowledgement

The authors are grateful to the UGC, New Delhi, for the research grant support and to Higher Education Department, Government of Gujarat for awarding the research scholarship to one of the authors (PHS).

References

- 1 Stolzer M, Stordeur M, Sobotta H & Riede V, *Phys Status Solidi B*, 138 (1986) 259
- 2 Arivuoli D, Gnanam F D & Ramasamy P, *J Mater Sci Lett*, 7 (1988) 711
- 3 Rowe D M & Bhandari C M, *Modern thermoelectronics*, (Holt Rinehart and Winston, London), 1981, p 103
- 4 Watanabe K, Sato N & Miyaoka, *J Appl Phys*, 54 (1983) 1256
- 5 Atakulov Sh B, Azimov T & Shamsiddinov A N, *Sov Phys Semicond*, 16 (1982) 1326
- 6 Goodman C H L, *Mater Res Bull*, 20 (1985) 237.
- 7 Jansa L, Lostak P, Sramkova J & Horak J, *J Mater Sci*, 27 (1992) 6062.
- 8 Roy B, Chakraborty B R, Bhattacharya R & Dutta A K, *Solid State Commun*, 25 (1978) 937
- 9 Jeon H W, Ha H P, Hyun D B & Shim J D, *J Phys Chem Solids*, 52 (1981) 579
- 10 Sakai N, Kajiwara N, Takemura T *et al*, *Solid State Commun*, 40 (1981) 1045
- 11 Sagar A & Faust J R J W, *J Appl Phys*, 38 (1967) 482
- 12 George J & Pradeep B, *Solid State Commun*, 56 (1985) 117
- 13 Rahman Khan M S & Akhtaruzzaman M, *Indian J Pure & Appl Phys*, 20 (1982) 656.
- 14 Testardi L R & Burstein E, *Phys Rev B*, 6 (1972) 460
- 15 Guha Thakurta S R & Bose A K, *Indian J Phys*, 44(1970)601
- 16 Desai C F & Soni P H, *Phys Semicond Dev*, 2 (1998) 1174
- 17 Bhatt V P, Patel R M & Desai C F, *Cryst Res Technol* 18 (1983) 1173
- 18 Buckle H, *Rev Metal*, 48 (1951) 957
- 19 Pandya N S, Bhatt V P, Vyas A R & Pandya G R, *Indian J Pure & Appl Phys*, 15 (1977) 750
- 20 Mott B W, *Micro-indentation hardness testing* (Butterworths Scientific Publications, London), 1956 Ch 1
- 21 Jani T M, Pandya G R & Desai C F, *Cryst Res Technol*, 29 (1994) 1
- 22 Vyas S M, Pandya G R & Desai C F, *Indian J Pure & Appl Phys*, 33 (1995) 191
- 23 Braunovic M, *The science of hardness testing and its research applications*, eds J H Westbrook and H Conrad (ASN, Ohio 1973) P 329
- 24 Meyer L., in *Micro-indentation hardness testing* (Butterworths Scientific Publications, London), 1956, Ch 4